

**Numerical Heat Transfer-Part A (USA)**

<https://www.tandfonline.com/toc/unht20/current>

*Accepted March 14<sup>th</sup>, 2024.*

**MHD PERISTALTIC TWO-PHASE WILLIAMSON NON-NEWTONIAN FLOW THROUGH THE URETERAL TUBE WITH MICROLITHS: ELECTROMAGNETIC THERAPY SIMULATION**

**P. Deepalakshmi<sup>1</sup>, E. P. Siva<sup>1,\*</sup>, D. Tripathi<sup>2</sup>, O. Anwar Bég<sup>3a</sup> and S. Kuharat<sup>3b</sup>**

<sup>1</sup> *Department of Mathematics, College of Engineering and Technology, SRM Institute of Science and Technology, Kattankulathur – 603203, Tamil Nadu, India.*

<sup>2</sup> *Department of Mathematics, National Institute of Technology, Uttarakhand-246174, India.  
dtripathi@nituk.ac.in*

<sup>3a</sup> *Professor/Director and* <sup>3b</sup> *Lecturer in Aeronautical Engineering, Multi-Physical Engineering Sciences Group, Dept. Mechanical and Aeronautical Engineering, Corrosion/Coatings Lab, 3-08, SEE Building, Salford University, Manchester, M54WT, UK. [O.A.Beg@salford.ac.uk](mailto:O.A.Beg@salford.ac.uk); [S.Kuharat2@salford.ac.uk](mailto:S.Kuharat2@salford.ac.uk)*

<sup>\*</sup> *Corresponding Author E. Mail Id: [sivae@srmist.edu.in](mailto:sivae@srmist.edu.in)*

## Abstract

The ureter typically experiences a frequency of one to five peristaltic contractions per minute. However, it is important to note that these contractions can be disrupted by various physical and mechanical irritants. Ionic contents in the urine make it electrically conducting and responsive to electromagnetic body forces. MHD can be deployed in biomagnetic therapy to control or mitigate symptoms associated with peristaltic pumping in the urinary system. This article therefore focuses on hydromagnetic effects on flow patterns of urine with debris (monoliths). The mechanism of urine flow is largely coordinated by the kidneys. The flow inside the ureter is interrupted by microliths which is generated by the sedimentation of excretory products. To simulate this, a two-phase formulation is adopted comprising the electromagnetic urological viscous fluid phase and particulate phase for solid grains. The peristaltic propulsion of two-phase liquid in the ureter is simulated as a sinusoidal wave propagation of incompressible non-Newtonian fluid. The Williamson viscoelastic model is deployed for the rheology. Heat transfer is also included with Soret thermo-diffusion and viscous heating effects. Long wave and low Reynolds number approximations are employed based on lubrication theory. The mass, momentum, energy and concentration conservation equations with associated boundary conditions are rendered non-dimensional via appropriate scaling transformations. A numerical solution is achieved via BVP4C MATLAB quadrature. Graphical visualizations of the velocity, temperature and concentration (solid grains) are given for the influence of suspension parameter ( $\zeta$ ), Hartmann number ( $M$ ), Prandtl Number ( $Pr$ ), Weissenburg number ( $We$ ), particle volume fraction ( $C$ ), Eckert number ( $Ec$ ), Soret number ( $Sr$ ), Schmidt number ( $Sc$ ). *The novelty of the present work is therefore the simultaneous consideration of a generalized two-phase model, wall slip, non-Newtonian characteristics, cross diffusion, viscous dissipation, mass diffusion, magnetic body force and curvature effects in peristaltic urological transport, which has not been undertaken previously.* The detailed simulations reveal that the flow velocity is reduced due to the presence of solid particles and the channel curvature, in comparison to the flow in an unobstructed channel devoid of solid particles. Enhancing the hydrodynamic slip parameter speeds up the movement of particles and fluid near the channel walls, boosts wall skin friction, raises pressure difference in the pumping area, and amplifies bolus magnitudes. The rise in peristaltic pumping results in a reduction in solid particle concentration, which is significant phenomena. This theoretical approach may aid in treating conditions such as Urinary Tract Infections (UTIs). The computations effectively demonstrate that significant manipulation in urological pumping characteristics can be achieved with electromagnetic field. Some new features of two-phase ureteral dynamics are highlighted of relevance to magnetic therapy techniques which will be beneficial to clinicians.

**Keywords:** *Biomagnetic therapy, Computational urological fluid dynamics, Concentration, Heat transfer, Monoliths, non-Newtonian, Numerical, Peristalsis, Soret thermo-diffusion, Trapping Bolus, Ureter flow, Viscous heating.*

## **Culminations**

- ❖ A detailed new formulation is given for magnetohydrodynamic (MHD) two-phase Williamson non-Newtonian ureteral transport with mass diffusion, Soret cross diffusion, viscous heating and peristaltic wave propulsion.
- ❖ We compute numerically the pressure gradient, skin friction, Nusselt number, and wall shear stress in a planar channel with flexible walls, which serves as a model for the ureter under a transverse magnetic field.
- ❖ We also investigate the impact of Hartmann number and Weissenberg non-Newtonian number on fluid and particle phase velocities.
- ❖ The present work reveals some interesting insights into electromagnetic ureteral peristaltic multi-phase non-Newtonian thermo-solutal transport phenomena via extensive visualization.
- ❖ There is a strong suppression in the ureteral fluid phase velocity for greater magnetic field confirming the excellent flow control abilities of Magnetic Ureteral Therapy (MUT).

## **1.Introduction**

Two-phase flows arise in numerous applications in medicine and technology. These flows are characterized by particles suspended in a viscous medium. Examples of applications include ventricular assist devices (VADs) also called blood pumps [1], magnetic pharmacology [2], lymphedema and transport in the swollen lymphatic nodes [3], bio microfluidic separation devices [4], orthopaedic biofluid dynamics [5], tissue transdermal transport [6], capillary filtration [7], dialysis treatments [8], interstitial flows [9], nanoparticle transport in asthmatic therapy [10], hazardous biowaste conveyance [11], interfacial hydrodynamics in blood flows [12] and synovial hydrodynamic lubrication [13]. As noted, two-phase flow applications are growing in 21<sup>st</sup> century microfluidics, which is the study of fluid flow in small channels and devices, wherein it may be deployed for manipulating and analysing cells and particles. During MRI the injection of a contrast agent into the blood stream also creates a two-phase system. Another complex and significant application of two-phase flows in medical fluid dynamics is the propulsion of urine in the ureter i.e. urodynamic transport. When contaminants and pathogen infect the ureter, sedimentation of particles in urological fluids can precipitate serious

disorders including alluviation calculi in the ureter [14]. While in the majority of patients with a normal urinary tract and kidney function, and no predisposing co-morbidities, urinary tract infections (UTIs) can often be self-limiting or readily cleared with a short course of antibiotics. However approximately 25% [15, 16] of UTI patients, however, experience persistent or recurrent infection and/or treatment failure, and complicated UTIs carry an increased likelihood of such outcomes. These complications have motivated scientists and engineers to utilize simulation models to investigate the mechanics of ureteral infection and how to combat the associated negative effects. The essential mechanism underlying urological transport is *peristalsis*. This is a complex rhythmic motion produced by successive waves of contraction in elastic, tubular structures which push their fluid or fluid-like contents forward. Peristalsis achieves exceptional efficiency in the urinary system there creates an involuntary sinusoidal muscular shrinkage of the uterine wall which push the urine from the kidneys to the urinary bladder via synergized wavy wall motions of the ureter controlled by electrical impulses. This mechanism is one of the most effective in nature for internal propulsion featuring also in embryonic heart development, pulmonary circulation, swallowing, digestive mixing, lymphatic dynamics etc. It also features prominently in external locomotion in snakes, eels, earthworms etc. Although many extensive investigations of peristalsis have been conducted by biologists for over a century, it was only in the late 1960s that engineers began to develop mathematical hydrodynamic models and experimental simulations of peristaltic propulsion. The seminal contributions of Fung and co-workers at UC San Diego [17] and Shapiro and co-workers at MIT [18], introduced the lubrication approximation for formulating peristaltic flow problems. This approach transforms the transient fixed frame scenario to a laboratory (moving) frame and assumes very low Reynolds numbers and high wave lengths for the peristaltic motion. It therefore dramatically simplifies the Navier-Stokes 3-D viscous flow model to axisymmetric flow in an infinitely long distensible tube. These studies produced comprehensive solutions for ranges of peristaltic motion depending on pressure difference and plotted streamlines, velocity distributions and also bolus characteristics. This approach was adopted subsequently by Lykoudis [19] to analyse the ureteral pumping. Boyarsky and Weinberg [20] extended the work in [19] examining in detail the hydrodynamics of the ureteropelvic junction and conus (specialized components of the ureter) and observing that in peristaltic pumping, the bolus at this point does not influence the pressures, flows or volume above it significantly. Most of the subsequent work in this area followed a similar methodology until the 21<sup>st</sup> century when CFD (computational fluid dynamics) emerged as a feasible tool. Lozano [21] explored both numerically and experimentally the dynamics of ureteral peristaltic motion. He assumed

however a Newtonian model and using small wavenumbers, described regular perturbation expansions and identified local and global bifurcations in streamline patterns. He also computed particle paths and addressed local bifurcations and their topological modifications with dynamical system techniques. This study identified a triplet of unique hydrodynamic phenomena- backward (reflux) pumping, trapping and augmented flow and furthermore noted the presence of a number of stagnation points. Kiil [22] studied the response of dilatation in the ureteral wall during catheter insertion. Vahidi *et al.* [23] deployed ADINA FSI finite element software to compute the two-way fluid-structure interaction between the compliant ureteral wall and the surrounding urological Newtonian fluid. The wall stimulation was accommodated as a nonlinear contact mechanics problem, and time-dependent alterations in the ureteral wall intraluminal shear stress during peristalsis were computed. They gave comprehensive visualization of key characteristics including ureteral wall compliance influence on contraction wave velocity, quantity of contraction waves on the ureteral outlet flow, pressure difference between the ureteral inlet and outlet and also the peak amplitude of the contraction wave. They observed that much greater shear stress arises in the proximal part of the ureter relative to the distal or central locations. middle and distal parts. Furthermore, they demonstrated that greater hydromechanical efficiency is achieved for larger amplitudes of the contraction wave and that sub-optimal performance of the ureteropelvic junction precipitates significant urological reflux even when there is a very gradual initiation stage for the peristaltic contraction wave. Gómez-Blanco *et al.* [24] used a fluid-structure interaction simulation to study the optimal design of stents for ureteral peristaltic pumping. They scrutinized closely the interaction between urine flow and a double-J stented ureter and deployed a variety of nonlinear viscoelastic models for the quasi-incompressible and isotropic ureteral wall deformation. They noted that wall compliance has a key effect on the peak amplitude of the contraction wave and also the tensile stress in the ureteric wall.

The above simulations were confined to *single-phase Newtonian peristaltic pumping*. However, the presence of contaminants in urological fluids can produce multi-phase flows. Two-phase phenomena are common since sedimentary deposits in the form of particles may flow with the viscous urological base liquid. The resulting hydrodynamic problem therefore requires an appropriate fluid-particle suspension model. A very popular methodology was introduced by Caltech applied mathematician, Saffman [25] in the early 1960s which he termed a “dusty fluid”. In this approach, suspended particles are studied as spherical rigid bodies and interfacial momentum transfer is possible. Marble [26] generalized the Saffman model to consider thermal effects and also other forms of slip. These models have been deployed

extensively in biological fluid dynamics in addition to other areas of complex industrial suspension rheology. Srivastava *et al.* [27] studied peristaltic two-phase flow with the fluid-particle suspension model. They evaluated the results of velocity using momentum equations in both phases and made comparison between them. Their computations showed that there is a reduction of fluid velocity in axial direction when there is increment in the solute concentration. Kamal *et al.* [28] studied the hydrodynamic wall slip effect on fluid-particle suspension peristaltic pumping in a distensible two-dimensional channel under sinusoidal waves. They showed that the critical value of pressure gradient is comparatively lower when particles are present relative to purely single-phase viscous Newtonian fluid. Many other studies have been communicated in peristaltic two-phase fluid dynamics addressing a variety of multi-physics effects including coupled thermal solutal transport [29], wall damping [30], viscoplastic fluidity [31], nanofluids and tapered conduit geometries [32], curved tubes [33], couple stress and thermal slip effects [34] and mass diffusion [35]. All these studies have revealed the significant influence of particle suspensions on peristaltic flow characteristics.

In recent times, a new therapy for ureteral infections has emerged. This exploits the electrically-conducting nature of urological liquids which due to the presence of ions and other chemicals respond to external electrical and magnetic fields. Magneto-hydrodynamic ureteral therapy (MUT) has been shown to very effective in the treatment of monolith obstructions in both ureteral and gynaecological performance [36]. Impulse magnetic field (IMF) control can strategically be deployed to activate impulse activity of ureteral smooth muscles in over 60% of patients and thereby optimally manage ureterolith fragments. More recently pioneering work in biomagnetic therapy at Stanford university [37] has led to the creation of a new medical device, MagSToNE (Magnetic System for Total Nephrolith Extraction), which utilizes magnetization to remove kidney stones during ureteroscopy to maximize the stone-free rate and minimize operating time. This technique has proven to be far superior to existing approaches such as ureteroscopy, in which a ureteroscope is passed endoscopically up to the stone and a laser fiber is used to fragment/and or dust the stone. MagSToNE has achieved comparable success rates but with much shorter operating time as fragments. It is much less intrusive and portable and exploits a different approach to urological hydrodynamics, namely magneto-hydrodynamics (MHD) technology. The invention consists of two components, a small-diameter flexible magnetic wire (MagWIRE) and superparamagnetic particles with surface chemistries that bind to kidney stones. After a kidney stone is fragmented, a superparamagnetic particle solution is instilled through the ureteral access sheath and coats the fragments, rendering them magnetizable. The MagWIRE has been tested rigorously and can

enter through the ureteroscope or the access sheath and uses a unique magnetic configuration to generate a strong magnetic field to optimize the capture of stone fragment along the entire length of the wire. Furthermore, this device can be deployed multiple times in succession to extract all fragments of monoliths not retrievable with conventional therapies. It is compatible with existing ureteroscopy setups and is set to revolutionize urological disorder treatments around the world.

Motivated by the afore-said magnetohydrodynamic ureteral therapy devices, in the present study we generalize previous investigations to consider *peristaltic pumping in ureteral two-phase (fluid-particle suspension) with non-Newtonian and magnetohydrodynamic body force effects* [38]. Lorentz body force is included to simulate magnetohydrodynamic drag. The Saffman fluid-particle suspension model is adopted, and heat transfer is also considered as are Soret thermal diffusion and viscous dissipation effects [39]. The robust Williamson rheological model [40,41,60] is utilized to accommodate for *shear-thinning (pseudoplastic) and shear thickening (dilatant) behaviour* of the electrically conducting urological fluid-particle suspension. It is important to note that a number of other non-Newtonian studies have been reported in peristaltic pumping of relevance to ureteral dynamics with other rheological models. *Ajithkumar et al.* [62] explored the flexibility of walls by peristaltic pumping a bi-viscous Bingham nanofluid through a porous medium under convective boundary conditions by employing R-K based shooting technique. *Ajithkumar et al.* [63,64] addressed the movement of a magnetohydrodynamic Ree–Eyring nanofluid through a porous conduit along with considering activation energy and thermal radiation. *Vajravelu and Ajithkumar et al.*, [65,66] examined the peristaltic pumping of different nanofluids through lubrication approach. *Jagadesh* [67] studied convective peristaltic pumping of a Casson viscoplastic yield stress fluid across an inclined porous wavy channel by employing a regular perturbation technique. *Ajithkumar et al.* [68,69] studied the bioconvective peristaltic transport of a non-Newtonian nanofluid similar to Sutterby and Jeffrey across a porous symmetric channel with compliant walls. *Hina and Kayani et al.* [70,71] analyzed the peristaltic motion of a non-Newtonian nanofluid following the Carreau–Yasuda (CY) model in a compliant walled channel using Buongiorno's model without assuming constant diffusion coefficients. *Yasin et al.* [72] primarily address the peristaltic flow of a hybrid nanofluid including copper (Cu) and silver (Ag) nanoparticles with blood as the carrier fluid in a symmetrical channel. *Yasin et al.* [73] scrutinised a viscous-elastic (Maxwell) fluid with slip condition to analyse hemodynamic in arteries and capillaries, taking into account Hall current features. Long wave and low Reynolds number approximations are employed based on lubrication theory. The mass, momentum,

energy and concentration conservation equations with associated boundary conditions are rendered non-dimensional via appropriate scaling transformations. A numerical solution is achieved via BVP4C MATLAB quadrature. Graphical visualizations of the velocity, temperature and concentration (solid grains) are given for the influence of suspension parameter ( $\zeta$ ), Hartmann number ( $M$ ), Prandtl Number ( $Pr$ ), Weissenburg number ( $We$ ), particle volume fraction ( $C$ ), Eckert number ( $Ec$ ), Soret number ( $Sr$ ), Schmidt number ( $Sc$ ). The simulations demonstrate that significant manipulation in urological pumping characteristics can be achieved with electromagnetic field. Some new features of two-phase ureteral dynamics are highlighted of relevance to magnetic therapy techniques which may be beneficial to clinicians.

## 2. Mathematical model for magnetized ureteral two-phase rheological flow

The physical model to be investigated is depicted in **Figure 1.a**, with a rendition of the feed mechanism via the kidneys to the ureter depicted in **Figure 1.b**. Two-dimensional viscous fluid-particle suspension hydromagnetic peristaltic pumping with rheological, thermal and viscous heating effects is considered in a planar channel with distensible walls, as a model of the ureter under a transverse magnetic field. The following assumptions are considered in the formulation:

- Two-dimensional
- Incompressible laminar flow
- Cartesian co-ordinate system ( $X, Y$ )
- Non-Newtonian fluid (Williamson model)
- Sinusoidal wave along tapered channel with particles

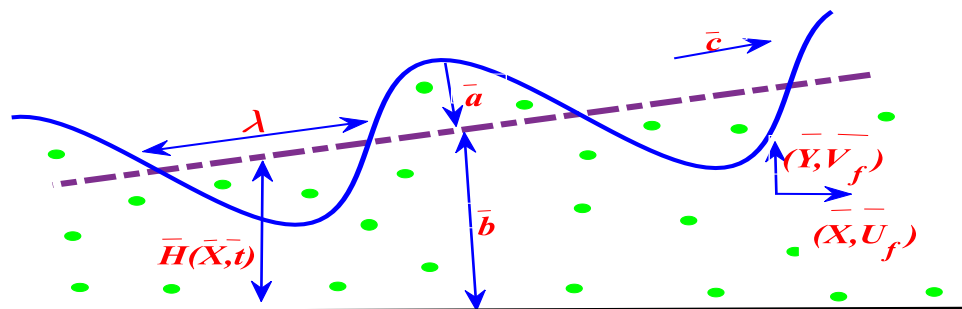


**Figure 1.a.** Schematic diagram of peristaltic ureteral MHD two-phase flow



**Figure 1.b.** The internal picture of kidney with ureteral stones

A sinusoidal wave of amplitude  $\tilde{a}$ ,  $\tilde{K}$  represents the channel length-dependent constant, wavelength  $\lambda$ , channel's half-width at the inlet is denoted by  $\tilde{b}$  and constant velocity  $\tilde{c}$  propagates along the channel wall with height  $\tilde{H}(\tilde{X}, \tilde{t})$  defined as:

$$\tilde{H}(\tilde{X}, \tilde{t}) = \tilde{a} \sin\left[\frac{2\pi}{\lambda}(\tilde{X} - \tilde{c}\tilde{t})\right] + \tilde{b} + \tilde{K}\tilde{X} \quad (1)$$

Magnetic induction, thermal dispersion, Dufour (diffuso-thermal) and thermal stratification effects are neglected. The magnetic field is sufficiently weak also to negate hall current effects. The governing conservation equations, i.e. fluid phase and particulate phase momentum, temperature, and concentration equations in an  $(\tilde{X}, \tilde{Y}, \tilde{t})$  coordinate system, amalgamating the models in [32, 33] and extending to include hydromagnetic effects can be shown to take the form:

**Fluid-Phase:**

$$\rho_f \left[ \tilde{U}_f \frac{\partial \tilde{U}_f}{\partial \tilde{X}} + \tilde{V}_f \frac{\partial \tilde{U}_f}{\partial \tilde{Y}} + \frac{\partial \tilde{U}_f}{\partial \tilde{t}} \right] = -\frac{\partial \tilde{P}}{\partial \tilde{X}} + \left( \frac{\partial \tilde{\tau}_{\tilde{X}\tilde{X}}}{\partial \tilde{X}} + \frac{\partial \tilde{\tau}_{\tilde{X}\tilde{Y}}}{\partial \tilde{Y}} \right) + \frac{SC}{1-C} (\tilde{U}_p - \tilde{U}_f) - \sigma B_0^2 \tilde{U}_f \quad (2)$$

$$\rho_f \left[ \tilde{U}_f \frac{\partial \tilde{V}_f}{\partial \tilde{X}} + \tilde{V}_f \frac{\partial \tilde{V}_f}{\partial \tilde{Y}} + \frac{\partial \tilde{V}_f}{\partial \tilde{t}} \right] = -\frac{\partial \tilde{P}}{\partial \tilde{Y}} + \left( \frac{\partial \tilde{\tau}_{\tilde{X}\tilde{Y}}}{\partial \tilde{X}} + \frac{\partial \tilde{\tau}_{\tilde{Y}\tilde{Y}}}{\partial \tilde{Y}} \right) + \frac{SC}{1-C} (\tilde{V}_p - \tilde{V}_f) \quad (3)$$

$$(1-C)(\rho c_p)_f \left[ \tilde{U}_f \frac{\partial \tilde{T}_f}{\partial \tilde{X}} + \tilde{V}_f \frac{\partial \tilde{T}_f}{\partial \tilde{Y}} + \frac{\partial \tilde{T}_f}{\partial \tilde{t}} \right] = (1-C)K \left( \frac{\partial^2 \tilde{T}_f}{\partial \tilde{X}^2} + \frac{\partial^2 \tilde{T}_f}{\partial \tilde{Y}^2} \right) + CS(\tilde{U}_f - \tilde{U}_p)^2 + \frac{\rho_p c_p C}{\omega_{\tilde{T}}} (\tilde{T}_p - \tilde{T}_f) \quad (4)$$

$$(1-C) \left[ \tilde{U}_f \frac{\partial \tilde{K}_f}{\partial \tilde{X}} + \tilde{V}_f \frac{\partial \tilde{K}_f}{\partial \tilde{Y}} + \frac{\partial \tilde{K}_f}{\partial \tilde{t}} \right] = (1-C) D_m \left( \frac{\partial^2 \tilde{K}_f}{\partial \tilde{X}^2} + \frac{\partial^2 \tilde{K}_f}{\partial \tilde{Y}^2} \right) + \frac{\rho_p C}{\rho_f \omega_{\tilde{K}}} (\tilde{K}_p - \tilde{K}_f) + \frac{D_m}{\tilde{T}_0} (1-C) K_{\tilde{t}} \left( \frac{\partial^2 \tilde{T}_f}{\partial \tilde{X}^2} + \frac{\partial^2 \tilde{T}_f}{\partial \tilde{Y}^2} \right) \quad (5)$$

In the aforementioned equations [40],

$$\tau_{\tilde{X}\tilde{X}} = 2(1+We\dot{\gamma}) \frac{\partial U}{\partial X}$$

$$\tau_{\tilde{X}\tilde{Y}} = (1+We\dot{\gamma}) \left( \frac{\partial U}{\partial Y} + \delta \frac{\partial V}{\partial X} \right)$$

$$\tau_{\tilde{Y}\tilde{Y}} = 2\delta(1+We\dot{\gamma}) \frac{\partial U}{\partial X}$$

$$\dot{\gamma} = \left( 4\delta^2 \left( \frac{\partial U}{\partial X} \right)^2 + \left( \frac{\partial U}{\partial Y} + \delta^2 \frac{\partial V}{\partial X} \right)^2 \right)^{1/2}$$

**Particle Phase:**

$$\rho_p C \left[ \tilde{U}_p \frac{\partial \tilde{U}_p}{\partial \tilde{X}} + \tilde{V}_p \frac{\partial \tilde{U}_p}{\partial \tilde{Y}} + \frac{\partial \tilde{U}_p}{\partial \tilde{t}} \right] = -C \frac{\partial \tilde{P}}{\partial \tilde{X}} + CS (\tilde{U}_f - \tilde{U}_p) \quad (6)$$

$$\rho_p C \left[ \tilde{U}_p \frac{\partial \tilde{V}_p}{\partial \tilde{X}} + \tilde{V}_p \frac{\partial \tilde{V}_p}{\partial \tilde{Y}} + \frac{\partial \tilde{V}_p}{\partial \tilde{t}} \right] = -C \frac{\partial \tilde{P}}{\partial \tilde{Y}} + CS (\tilde{V}_f - \tilde{V}_p) \quad (7)$$

$$\rho_p C c_p \left[ \tilde{U}_p \frac{\partial \tilde{T}_p}{\partial \tilde{X}} + \tilde{V}_p \frac{\partial \tilde{T}_p}{\partial \tilde{Y}} + \frac{\partial \tilde{T}_p}{\partial \tilde{t}} \right] = \frac{C \rho_p c_p}{\omega_{\tilde{T}}} (\tilde{T}_f - \tilde{T}_p) \quad (8)$$

$$\left[ \tilde{U}_p \frac{\partial \tilde{K}_p}{\partial \tilde{X}} + \tilde{V}_p \frac{\partial \tilde{K}_p}{\partial \tilde{Y}} + \frac{\partial \tilde{K}_p}{\partial \tilde{t}} \right] = \frac{1}{\omega_{\tilde{K}}} (\tilde{K}_f - \tilde{K}_p) \quad (9)$$

Where the subscripts  $f$  and  $p$  denote fluid phase and solid (particulate granules) phase, respectively. In Eqns. (2)-(9) the following notation applies:  $C$  is the partial volume fraction parameter,  $(\tilde{X}, \tilde{Y}, \tilde{t})$  are axial and transverse coordinates and time,  $\rho_f$  is Williamson urological

fluid density,  $\tilde{U}_f, \tilde{V}_f$  are axial and transverse fluid phase velocity components,  $\tilde{P}$  is pressure,  $\tilde{\tau}_{\tilde{x}\tilde{x}}$  and  $\tilde{\tau}_{\tilde{y}\tilde{y}}$  are the shear stress tensor components,  $\tilde{U}_p, \tilde{V}_p$  are axial and transverse particle phase velocity components,  $S$  is Stokes number,  $\sigma$  is electrical conductivity of the Williamson urological fluid and  $B_0$  is transverse magnetic field intensity,  $(\rho c_p)_f$  is specific heat capacity of the Williamson urological fluid,  $\tilde{T}_f$  is fluid phase temperature,  $K$  is thermal conductivity of the Williamson fluid (isotropic),  $\rho_p$  is particulate density,  $\omega_{\tilde{\tau}}$  is particle phase Saffman wall slip coefficient,  $\tilde{T}_p$  is particle phase temperature,  $\tilde{K}_f$  is particulate concentration,  $D_m$  is molecular diffusivity of the particles in urological Williamson fluid. The following dimensional boundary conditions [39] are prescribed at the channel walls ( $\tilde{Y} = 0 : \tilde{Y} = \tilde{H}$ )

$$\frac{\partial \tilde{U}_f}{\partial \tilde{Y}} = 0, \frac{\partial \tilde{T}_f}{\partial \tilde{Y}} = 0, \frac{\partial \tilde{K}_f}{\partial \tilde{Y}} = 0, \frac{\partial \tilde{U}_p}{\partial \tilde{Y}} = 0, \frac{\partial \tilde{T}_p}{\partial \tilde{Y}} = 0, \frac{\partial \tilde{K}_p}{\partial \tilde{Y}} = 0 \text{ at } \tilde{Y} = 0 \quad (10)$$

$$\tilde{U}_f = 0, \tilde{T}_f = \tilde{T}_h, \tilde{K}_f = \tilde{K}_h \text{ at } \tilde{Y} = \tilde{H} \quad (11)$$

The nonlinear boundary value problem defined by Eqns. (10)- (11) in primitive form is formidable to solve even with modern numerical methods. Also this requires explicit data for each fluid and particle property. To facilitate a solution, scaling transformations are therefore introduced. These dramatically simplify the problem at hand and simultaneously enable scaling of different thermal, magnetic and hydrodynamic effects via appropriate dimensionless numbers, a very powerful tool in fluid dynamics. Proceeding with the analysis, the following non-dimensional variables are invoked [32, 33, 34,40]:

$$\begin{aligned} X &= \frac{\tilde{X}}{\lambda}, Y = \frac{\tilde{Y}}{\tilde{a}}, U_f = \frac{\tilde{U}_f}{\tilde{c}}, U_p = \frac{\tilde{U}_p}{\tilde{c}}, V_f = \frac{\tilde{V}_f \lambda}{\tilde{a} \tilde{c}}, V_p = \frac{\tilde{V}_p \lambda}{\tilde{a} \tilde{c}}, P = \frac{\tilde{a}^2 \tilde{P}}{\mu \tilde{c} \lambda}, \\ \text{Re} &= \frac{\rho_f \tilde{a} \tilde{c}}{\mu}, \theta_f = \frac{\tilde{T}_f - \tilde{T}_0}{\tilde{T}_h - \tilde{T}_0}, \theta_p = \frac{\tilde{T}_p - \tilde{T}_0}{\tilde{T}_h - \tilde{T}_0}, h = \frac{\tilde{H}}{\tilde{a}}, \alpha_f = \frac{\tilde{K}_f - \tilde{K}_0}{\tilde{K}_h - \tilde{K}_0}, \alpha_p = \frac{\tilde{K}_p - \tilde{K}_0}{\tilde{K}_h - \tilde{K}_0}, \\ t &= \frac{\tilde{c} \tilde{t}}{\lambda}, \delta = \frac{\tilde{a}}{\lambda}, \tau_{xx} = \frac{\lambda \tilde{\tau}_{\tilde{x}\tilde{x}}}{\mu \tilde{c}}, \tau_{xy} = \frac{\tilde{a} \tilde{\tau}_{\tilde{x}\tilde{y}}}{\mu \tilde{c}}, \tau_{yy} = \frac{\tilde{a} \tilde{\tau}_{\tilde{y}\tilde{y}}}{\mu \tilde{c}}, \text{We} = \frac{\Gamma \tilde{c}}{\tilde{a}}, \dot{\gamma} = \frac{\tilde{\gamma} \tilde{a}}{\tilde{c}}, S = \frac{\mu \zeta}{\tilde{a}^2}, \\ \text{Ha} &= \sqrt{\frac{\sigma}{\mu} B_0 \tilde{a}}, \text{Ec} = \frac{\tilde{c}^2}{(\tilde{T}_h - \tilde{T}_0) c_p}, \text{Pr} = \frac{\mu c_p}{K}, \text{Sr} = \frac{D_m \rho_f K_{\tilde{T}}}{\mu \tilde{T}_0} \left( \frac{\tilde{T}_h - \tilde{T}_0}{\tilde{K}_h - \tilde{K}_0} \right), \text{Sc} = \frac{D_m \rho_f}{\mu} \end{aligned} \quad (12)$$

These parameters denote respectively the dimensionless  $(\tilde{X}, \tilde{Y})$  axial and transverse coordinates, non-dimensional axial fluid phase velocity, non-dimensional axial particulate phase velocity, dimensionless transverse particle phase velocity, dimensionless pressure, Reynolds number (based on wave amplitude and peristaltic wave speed), dimensionless fluid phase temperature function, dimensionless particulate phase temperature function, dimensionless height of channel (ureteral conduit), fluid concentration parameter, particulate concentration parameter, dimensionless time, amplitude to wave length ratio, non-dimensional shear stress components, Weissenberg number, shear rate, momentum Stokes number, Hartmann magnetic number, Eckert (viscous heating) number, Prandtl number, Soret number and Schmidt number. Saffman suspension parameter is denoted  $\xi$ . Implementing the transformations (12) in Eqns. (1)-(11), the transformed non-dimensional boundary value problem emerges as:

**Dimensionless Fluid phase:**

$$\frac{\partial P}{\partial X} = \frac{\partial^2 U_f}{\partial Y^2} \left[ 1 + 2We \left( \frac{\partial U_f}{\partial Y} \right) \right] + \frac{\zeta C}{1-C} (U_p - U_f) - (Ha)^2 U_f \quad (13)$$

$$\frac{\partial P}{\partial Y} = 0 \quad (14)$$

$$\left( \frac{\partial^2 \theta_f}{\partial Y^2} \right) + \frac{C Pr Ec}{1-C} \frac{1}{\zeta} \left( \frac{dP}{dX} \right)^2 = 0 \quad (15)$$

$$\left( \frac{\partial^2 \alpha_f}{\partial Y^2} \right) + Sr Sc \left( \frac{\partial^2 \theta_f}{\partial Y^2} \right) = 0 \quad (16)$$

**Dimensionless Particle phase:**

$$\frac{\partial P}{\partial X} = -\zeta (U_p - U_f) \quad (17)$$

$$\theta_f = \theta_p \quad (18)$$

$$\alpha_f = \alpha_p \quad (19)$$

**Dimensionless Boundary conditions**

$$\frac{\partial U_f}{\partial Y} = 0, \frac{\partial \theta_f}{\partial Y} = 0, \frac{\partial \alpha_f}{\partial Y} = 0, \frac{\partial U_p}{\partial Y} = 0, \frac{\partial \theta_p}{\partial Y} = 0, \frac{\partial \alpha_p}{\partial Y} = 0 \quad \text{at } Y = 0 \quad (20)$$

$$U_f = 0, \theta_f = 1, \alpha_f = 1 \quad \text{at } Y = h \quad (21)$$

Here the transformed wall equation is mentioned as,

$$h = 1 + \eta + d \sin 2\pi[X - t]$$

$$\text{Where} \quad \eta = \frac{\tilde{K}\tilde{X}}{a}, d = \frac{\tilde{b}}{a} < 1$$

The skin-friction coefficient, also known as the wall shear stress, is determined by applying equation (22). Similarly, the thermal flux, which represents the rate of thermal exchange, is determined by applying equation (23).

The skin friction parameter ( $C_f$ ) on the wall is precisely described as

$$C_f = -\mu \left( \frac{\partial U}{\partial Y} \right) \quad \text{at } Y = h \quad (22)$$

The local Nusselt number parameter ( $Nu$ ) is precisely defined as

$$Nu = - \left( \frac{\partial \theta}{\partial Y} \right) \quad \text{at } Y = h \quad (23)$$

The equation governing the rate of mass transfer through the wall is expressed as Sherwood number ( $Sh$ )

$$Sh = - \left( \frac{\partial \alpha}{\partial Y} \right) \quad \text{at } Y = h \quad (24)$$

### 3. MATLAB Numerical Solutions and Methodology

The above mentioned Linear ordinary differential equations (13 - 19) were solved numerically utilising MATLAB's bvp4c function, together with Equations (20) and (21) was associated with the boundary conditions.

To aid in the achievement of this resolution, the following procedures were implemented:

- ✓ System Reduction: The introduction of new variables led to the transformation of a complex set of higher-order partial differential equations into a simpler set of first-order ordinary differential equations.
- ✓ Generation of Boundary Conditions: To ensure adherence to the problem's constraints, boundary conditions were established for the variables that were recently incorporated.
- ✓ The suitable initial approximations for these newly introduced variables were ascertained, thereby providing a basis for the numerical resolution.
- ✓ By meticulously adhering to these procedures, the intended solution was achieved utilizing the `bvp4c` function, thereby successfully resolving the resulting system.

The second-order governing equations including both fluid and particle phases were transformed into a set of first-order ordinary differential equations through the inclusion of new variables. The variables  $U$  and  $U'$  were defined as  $f_1$  and  $f_2$ , respectively.  $\theta$  and  $\theta'$  were defined as  $f_3$  and  $f_4$ , while  $\alpha$  and  $\alpha'$  were defined as  $f_5$  and  $f_6$ , respectively. The procedure described the transformation of the original set of linked higher-order differential equations and their corresponding boundary conditions into a system of five first-order differential equations. The boundary conditions were adjusted to match the converted equations. The system of first-order linear ordinary differential equations generated is as follows:

$$U' = f_2 \quad (25)$$

$$U'' = f_2' = \frac{1}{[1 + 2We(f_2)]} \left[ (Ha)^2 f_1 + P \left( \frac{1}{1-C} \right) \right] \quad (26)$$

$$\theta' = f_4 \quad (27)$$

$$\theta'' = f_4' = -\frac{C Pr Ec}{1-C} \frac{1}{\zeta} P^2 \quad (28)$$

$$\sigma' = f_6 \quad (29)$$

$$\alpha'' = f_6' = -SrSc(f_4') \quad (30)$$

The associated boundary conditions are

$$f_a(2) = 0, f_a(4) = 0, f_a(6) = 0, \quad (31)$$

$$f_b(1) = 0, f_b(3) = 1, f_b(5) = 1 \quad (32)$$

A numerical solution is achieved via BVP4C MATLAB quadrature. This technique has been applied to many multi-physical fluid dynamics problems e. g. triple diffusive convection duct flows [45], robotic smart lubrication films [46], bio magnetic hypodermic coating flows [47],

carbon wall nanotube bio-coatings [48], ternary hybrid nanofluid magnetic functional coatings [49] and electromagnetic squeezing tribological applications [50, 51]. It can accommodate any order of derivatives. In MATLAB this quadrature is used to obtain solutions for the fluid and particulate velocity functions, temperature functions and concentration function. BVP4C uses stepping formulae which are summarized in [47]. Further details are given in Kattan [52]. The algorithm relies on an iteration structure. BVP4C is a numerical platform that implements the Lobato IIIa three-stage formula. This is a collocation formula which is formed by a polynomial collocation. It provides a C1-continuous solution that is fourth-order accurate uniformly in  $x \in [a, b]$ .

The fourth-order formulae are given below:

$$k_1 = L f(x_n, y_n) \quad (33)$$

$$k_2 = L f\left(x_n + \frac{L}{2}, y_n + \frac{k_1}{2}\right) \quad (34)$$

$$k_3 = L f\left(x_n + \frac{L}{2}, y_n + \frac{k_2}{2}\right) \quad (35)$$

$$k_4 = L f(x_n + L, y_n + k_3) \quad (36)$$

$$y_{n+1} = y_n + \frac{k_1}{6} + \frac{k_2}{3} + \frac{k_3}{3} + \frac{k_4}{6} + O(L^5) \quad (37)$$

where  $L = (x_{i+1} - x_i)$  represents the size of each subinterval. The crucial part in utilizing `bvp4c` is the variation step and early guessing of the mesh point. Besides, the efficiency will eventually depend on the programmer ability in providing the algorithm with an initial guess for the solution. Two folders can be created, for example, namely, “code a” and “code b”, for the trial-and-error initial guess and continuous iterations that approximate closely to the initial guess, respectively. The above-described computing approach cannot be used without transforming the higher-order differential equations to differential equations of order one. Some commands in handling the function such as “`@odeBVP`” and “`@odeBC`” are from the syntax of the solver “`sol = bvp4c`” (`@OdeBVP`, `@OdeBC`, `solinit`, `options`). The iterative process is carried out until an accuracy of  $10^{-6}$  is achieved which is obtained for the values of the boundary conditions and step size. The numerical results obtained from the solver are then plotted as graphs.

## 4. MATLAB results and discussion

Extensive computations have been conducted in MATLAB to determine the influence of all key control parameters on the peristaltic multi-physical transport problem. Specifically these parameters are Saffman suspension parameter ( $\zeta$ ), Hartmann number ( $M$ ), Prandtl Number ( $Pr$ ), Weissenburg number ( $We$ ), particle volume fraction ( $C$ ), Eckert number ( $Ec$ ), Soret number ( $Sr$ ) and Schmidt number ( $Sc$ ). The effects of these parameters on fluid/particle velocity functions, fluid/particulate temperature function and particulate concentration function are depicted in **Figures. 2- 13**. All data utilized is extracted from clinically viable sources [53-55] and earlier studies [42]. Velocity, temperature and concentration are considered in turn.

### 4.1. Velocity Characteristics

**Figure 2** shows that a significant decrement in both fluid and particle phase velocity is induced with elevation in Hartmann magnetic number ( $M$ ). The major reason for the reduction in fluid phase velocity is due to the action of Lorentz force on the electrically conducting non-Newtonian urological liquid. This arises in the linear retarding body force term in Eqn. (13),  $-(Ha)^2 U_f$ . The influence of magnetic field generates a strong resistance to the axial flow which induces deceleration. The urological volumetric flow rate which is proportional to velocity will also be suppressed. Higher Hartmann number therefore achieves excellent flow control via a non-intrusive means which has been shown to be beneficial in urological disorders [37, 38]. By virtue of the definition of  $Ha = \sqrt{\frac{\sigma}{\mu}} B_0$ , expresses the relative influence of the Lorentzian magnetic force to the viscous force in the regime. When  $Ha = 1$  both forces contribute equally, and Hartmann-Stokes boundary layers may arise at the interior of the ureteral duct. When  $Ha = 0$  magnetic effects vanish, and the urological liquid is electrically non-conducting. When  $Ha > 1$  the magnetic force dominates the viscous force, and this effectively stifles momentum development in the duct. The range of magnetic field intensities studied here is representative of the actual magnitudes explored in [35]. In all the profiles peak velocity magnitude is computed at the duct centreline ( $Y = 0$ ) since only the upper duct half space region is plotted due to symmetry (the actual duct depth extremities extend over the range,  $-1 < Y < 1$ ). The opposing force augmented the non-Newtonian potency of the reactive Williamson fluid and diminished the heat generation within the system. Consequently, the

viscosity of the fluid is enhanced as the molecular bond is stimulated throughout the flow regime. It is discovered that a greater transverse magnetic field, represented by an increasing Hartmann number, similar retardation may be found for both fluid and particle.

**Figure 3** reveals the response in velocity with an alteration in Saffman suspension parameter,  $\zeta$ . This parameter features in the *momentum Stokes number*,  $S = \frac{\mu\zeta}{\bar{\alpha}^2}$ , and arises in the fluid phase-particulate phase coupling term,  $+\frac{\zeta c}{1-c}(U_p - U_f)$  in the fluid phase momentum eqn. (13). Contrary to the Lorentzian drag term, the coupling term is an assistive body force and accentuation in the parameter,  $\zeta$  implies greater slip between the fluid and particles leading to an acceleration in the fluid phase. The suspension of granules accelerates with enhancement of average velocity of particles. A significant decrease in axial particle phase velocity is observed. Both phases are presented here with opposite results.

**Figure 4** Illustrates the evolution in fluid and particle phase velocity with increasing Weissenberg number ( $We$ ). This parameter arises uniquely in the modified shear term,  $+2We \left(\frac{\partial U_f}{\partial Y}\right) \left(\frac{\partial^2 U_f}{\partial Y^2}\right)$  in Eqn. (13) which is a mixed derivative term. The *Weissenberg number* ( $We$ ) embodies the relative contribution of the elastic forces to the viscous forces in the rheological urinary fluid. It also expresses the ratio of stress relaxation time of the fluid to the specific process time. It is most deployed for simple shear flows where it also describes the product of the shear rate and the relaxation time. When  $We = 0$  non-Newtonian effects vanish since elastic effects swamp out viscous effects. Since all rheological liquids including magnetic urological fluids are *elastico-viscous*, they combine elastic and viscous properties. For situations wherein the relaxation time of a flow is much less than the timescale of an elastic-viscous fluid, then viscous effects dominate. Conversely when relaxation time of the flow exceeds the timescale, elastic effects will be amplified over viscous effects. The Weissenberg number can also be regarded as the inverse Deborah number (ratio of the time scale of the flow and the stress relaxation time).

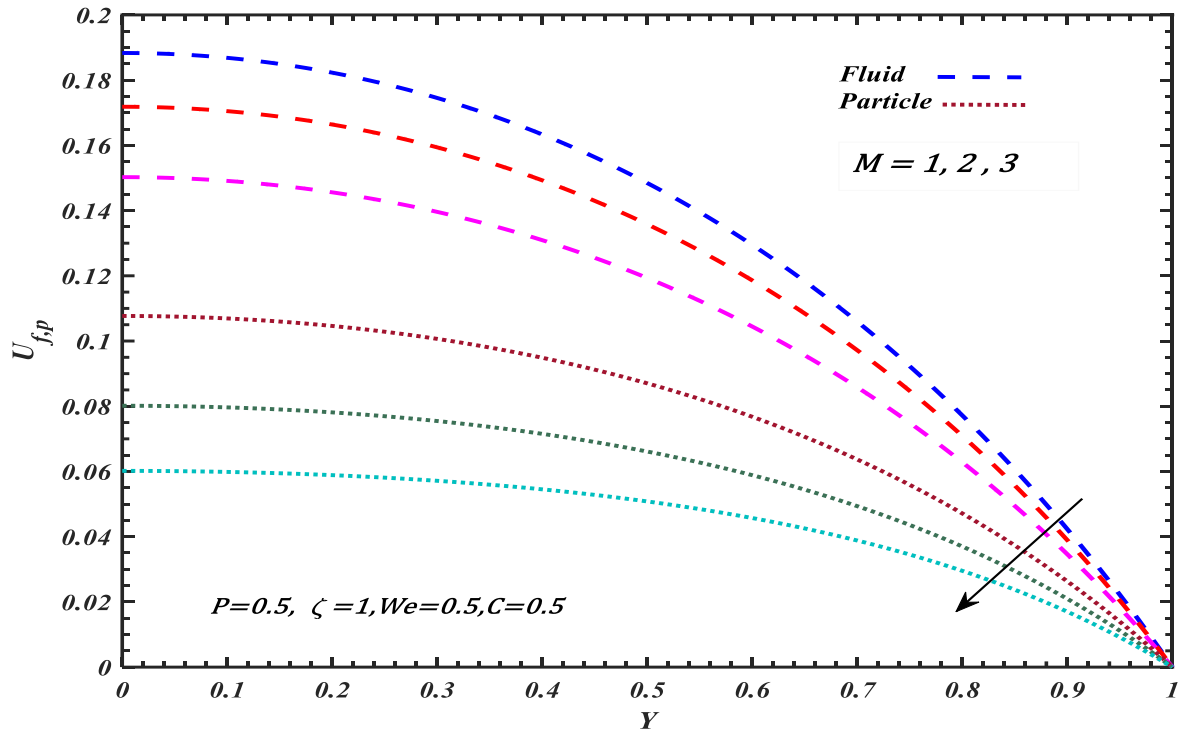


**Figure 2.** Impact of Hartmann number ( $M$ ) on fluid and particle phase velocity ( $U_{f,p}$ )

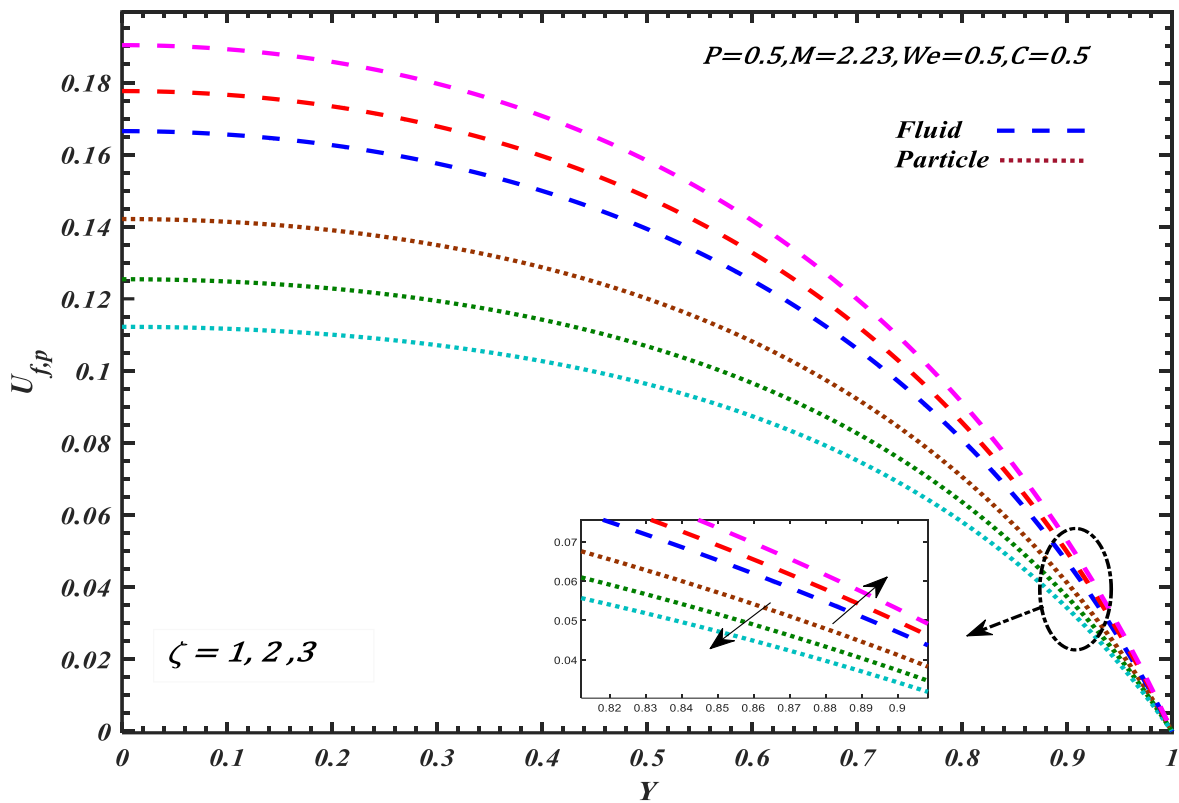


**Figure 3** Impact of Saffman suspension parameter on fluid and particle phase velocity ( $U_{f,p}$ )

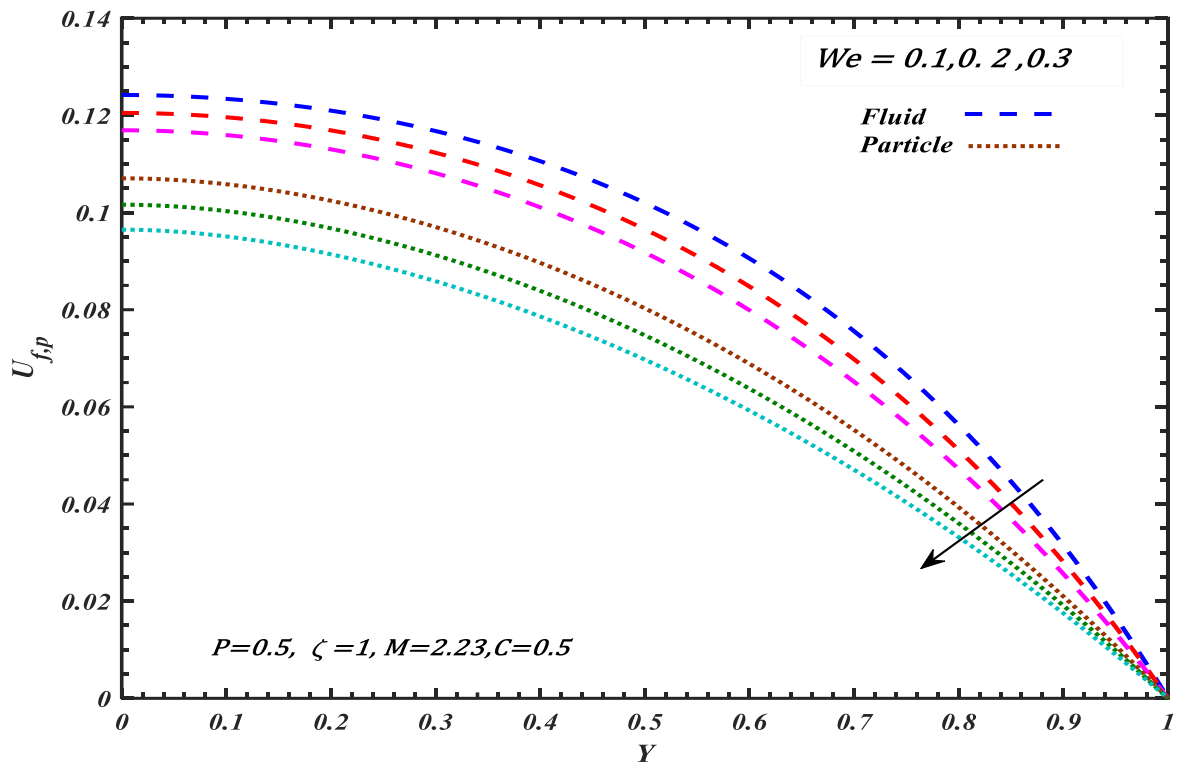


**Figure 4** Impact of Weissenberg number ( $We$ ) on fluid and particle phase velocity ( $U_{f,p}$ )

It is evident that as Weissenberg number increases the viscous forces increases relative to the elastic forces which induces strong deceleration in urological fluid (tensile stresses related to the first normal stress difference are reduced which contributes significantly to this process). It also slows down the movement of particles. The Weissenberg number in rheology also computes the degree of anisotropy or orientation generated by the fluid deformation and is relevant for constant stretch history flows as studied here. In cases where non-constant stretch history arises e.g. complex polymers in bionics, it is more appropriate to deploy the Deborah number which better expresses physically the rate at which elastic energy is stored or released in the fluid.

#### 4.2. Temperature Characteristics

**Figure 5** visualizes the impact of Prandtl number ( $Pr$ ) on fluid phase temperature. Prandtl number expresses the relation between momentum diffusivity and thermal diffusivity. It is also an inverse function of thermal conductivity of the urological fluid. A strong decrement is induced in temperature in the fluid phase. Higher Prandtl number fluids diffuse thermal energy (heat) much less efficiently than lower Prandtl number fluids. The values for rheological urological fluid are closer to water ( $Pr \sim 7$  at room temperature). Prandtl number also can be used to quantify the relative thickness of the momentum and thermal boundary layers

developing at the ureteral tube internal walls. When Prandtl number equals unity the momentum and energy diffusion rates are equivalent in the peristaltic regime. However, for Prandtl number in excess of unity the momentum diffusion rate greatly exceeds the thermal diffusion rate. This certainly applies in the present case of ureteral hydrodynamics [53-55]. The influence of particle volume fraction ( $C$ ) on fluid phase temperature is depicted in **Figure 6**. Peak temperature always arises at the ureteral tube centre line. It vanishes at the upper wall ( $Y = 1$ ). As the percentage of monolith particles increases, the thermal convection process is inhibited. The parameter  $C$  features in both the fluid phase momentum eqn. (13) as  $+\frac{\zeta C}{1-C}(U_p - U_f)$  and also in the fluid phase temperature eqn. (15) as the term,  $+\frac{C Pr Ec}{1-C} \frac{1}{\zeta} \left(\frac{dP}{dX}\right)^2$ . It clearly has a detrimental effect on temperature as it appears in the denominator ( $1-C$ ) and therefore elevation in  $C$  reduces the thermal diffusion in the fluid phase and manifests in a depletion in temperatures across the upper half space of the duct. Even a minor enhancement in volume fraction from 10% ( $C = 0.1$ ) to 12% ( $C = 0.12$ ) has a dramatic effect on thermal distributions in the urological fluid. The volumetric heat capacity of the monolith granule particles is enhanced with volume fraction which boosts thermal conduction in the suspended particles but counteracts heat diffusion in the urological base fluid [53]. **Figure 7** illustrates the influence of Eckert number ( $Ec$ ) on temperature parameter. Eckert number characterizes the viscous heating in the urological fluid which is attributable to internal friction at the molecular level. The friction induced generates thermal energy which energizes the urological fluid and boosts temperatures. Internal friction alters the viscosity of the urological fluid which also contributes to a temperature change since via the Prandtl number there will be a modification in momentum diffusion rate relative to thermal diffusion rate due to viscous heating. The rate of change of temperature with height of the duct is also elevated as Eckert number increases (i.e. a steeper gradient is produced). **Figure 8** visualizes the impact of the Saffman suspension parameter ( $\zeta$ ) on temperature evolution in the ureteral duct. There is a clear accentuation in fluid phase temperature as the suspension parameter is elevated. The slip effect between particles and the base urological fluid is encouraged with higher values of this parameter. This intensifies the micro-convection round the suspended particles which contributes to enhanced thermal diffusion in the base fluid and the resulting enhancement in temperature. Monotonic decays are computed consistently from the duct centreline to the upper wall, and no cross-over in profiles is witnessed.

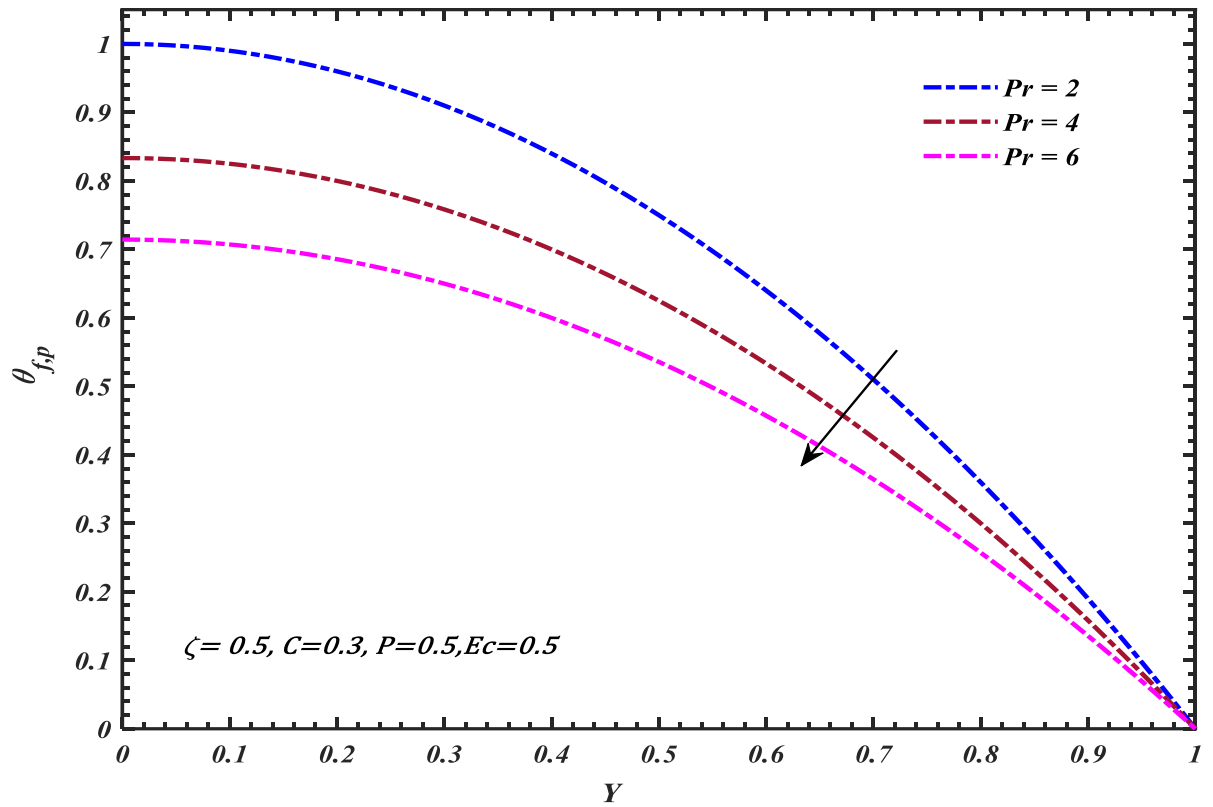


**Figure 5.** Impact of Prandtl number ( $Pr$ ) on fluid and particle phase velocity temperature  $(\theta)_{f,p}$

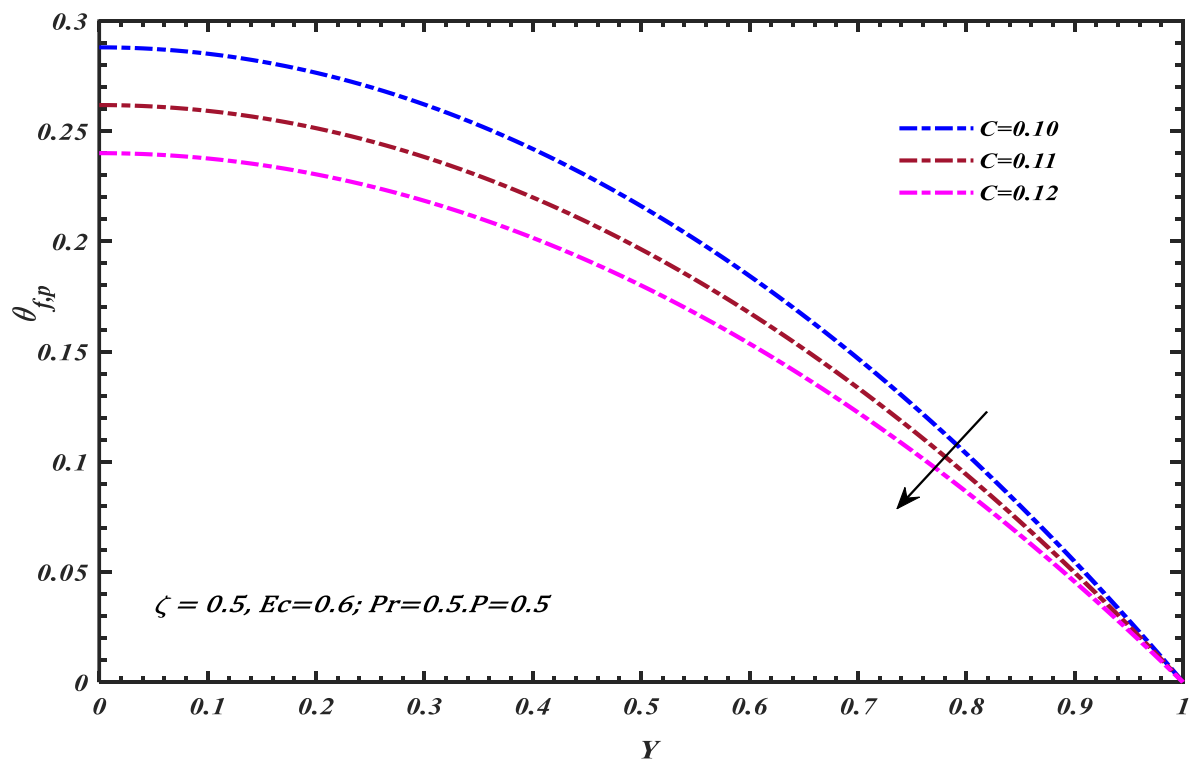


**Figure 6.** Impact of particle volume fraction ( $C$ ) on fluid and particle phase temperature  $(\theta)_{f,p}$

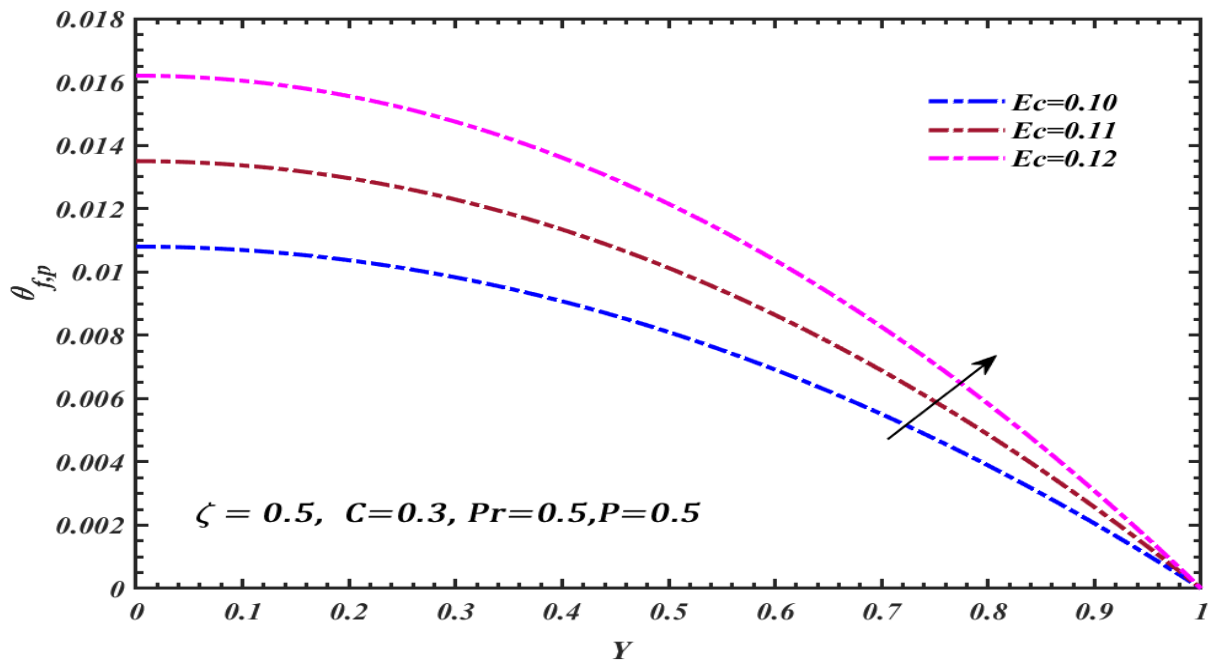


**Figure 7.** Impact of Eckert number ( $Ec$ ) on fluid and particle phase temperature  $(\theta)_{f,p}$

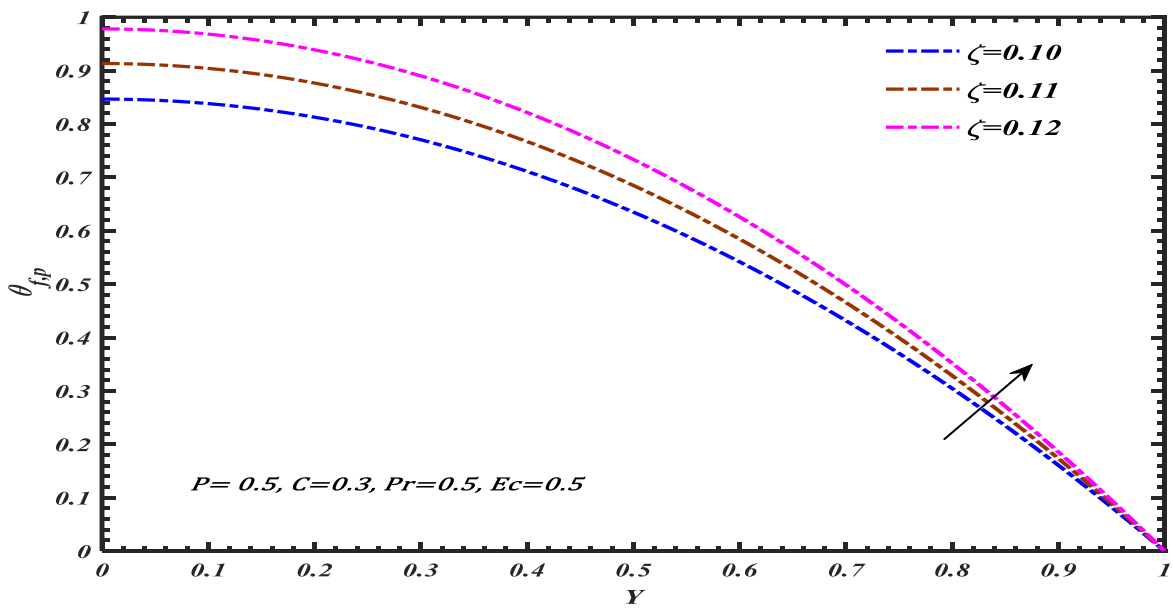


**Figure 8.** Impact of Saffman suspension parameter ( $\zeta$ ) on fluid and particle phase temperature  $(\theta)_{f,p}$

#### 4.3. Suspended particle concentration characteristics and Pressure gradient

In this final section of the discussion, we address the impact of selected control parameters on the particulate concentration. This is distinct from the volume fraction ( $C$ ) which relates to the percentage volume of suspended particles in the urological fluid. The

interconnection between suspension parameter ( $\zeta$ ) and concentration in peristaltic flow exhibits a high degree of complexity and is subject to the influence of multiple factors which is depicted in **Figure 9**. The dimensions and morphology of suspended particles exert a significant influence. Particles that are larger in size or have irregular shapes may exhibit distinct interactions with the fluid and the ureteral tube walls in comparison to smaller, spherical particles, resulting in differences in the flow and mass transfer characteristics. The findings indicate that there is an inverse relationship between the distribution of suspension parameter and concentration i.e. larger values of the Saffman suspension parameter ( $\zeta$ ) produce a depletion in concentration magnitudes. **Figure 10** visualizes the influence of Schmidt number ( $Sc$ ) on the concentration of the particles suspended in the urological fluid. The Schmidt number represents the relative rates of mass diffusion and momentum diffusion inside the peristaltic regime. A high Schmidt number signifies that the rate of momentum diffusion is greater than that of mass diffusion. Hence, the concentration is suppressed with increment in Schmidt number. The sub-unity values of  $Sc$  in **Figure 10** are representative of actual urological contamination with monoliths [see for example, 55, 56]. A similar effect on the concentration profile (**Figure 11**) is noticed with variation in the thermo-diffusive parameter i.e. Soret number  $Sr$ . This parameter also features in the same term as the Schmidt number, viz,  $+SrSc \left( \frac{\partial^2 \theta_f}{\partial Y^2} \right)$  in the fluid phase temperature eqn. (16). When the Soret number increases from zero, this indicates that thermal diffusion is the dominant mechanism. Concentration magnitudes clearly diminish with magnifying the values of Soret number ( $Sr$ ). The term “concentration” in the context of peristaltic flow often pertains to the existence of solutes or particles inside the fluid. The distribution of concentration within the tube may exhibit variations due to the influence of other mixing and transport phenomena. This effect is observed in **Figure 12** as a decrease in the fluid concentration profile is computed with increasing values of viscous dissipation parameter, Eckert number ( $Ec$ ). This parameter features, as noted earlier, in the fluid phase temperature eqn. (15), specifically the term,  $+\frac{C Pr Ec}{1-C} \frac{1}{\zeta} \left( \frac{dP}{dX} \right)^2$ . The correlation between particle concentration and particle volume fraction is contingent upon the characteristics of both the particles and the fluid in which they are immersed. **Figure 13** shows that with all other variables being constant, the increase in the number of particles in the urological fluid i.e. volume fraction,  $C$ , substantially enhances the concentration in the fluid. **Figure 14** gives various values of the Weissenberg number ( $We$ ) with  $a = 0.5$ ,  $b = 0.5$ ,  $d = 1$ , and  $C = 0.6$ . The study reveals that the rate of change of pressure with respect to distance ( $dP/dX$ ) falls as the

Weissenberg number ( $We$ ) increases. The pressure gradient is significantly reduced in Figure 15 and significantly increased in Figure 16. In these figures, positive values of  $(dP/dX)$  are maintained for all  $x$  values, indicating the absence of a reverse pressure gradient. This is a key feature of peristaltic pumping and is highly beneficial for enhancing the efficiency of MHD ureteral therapy in biomedical engineering. The magnetic field boosts the peristaltic flow, leading to significant changes in pressure distributions due to the inverse relationship between velocity and pressure.

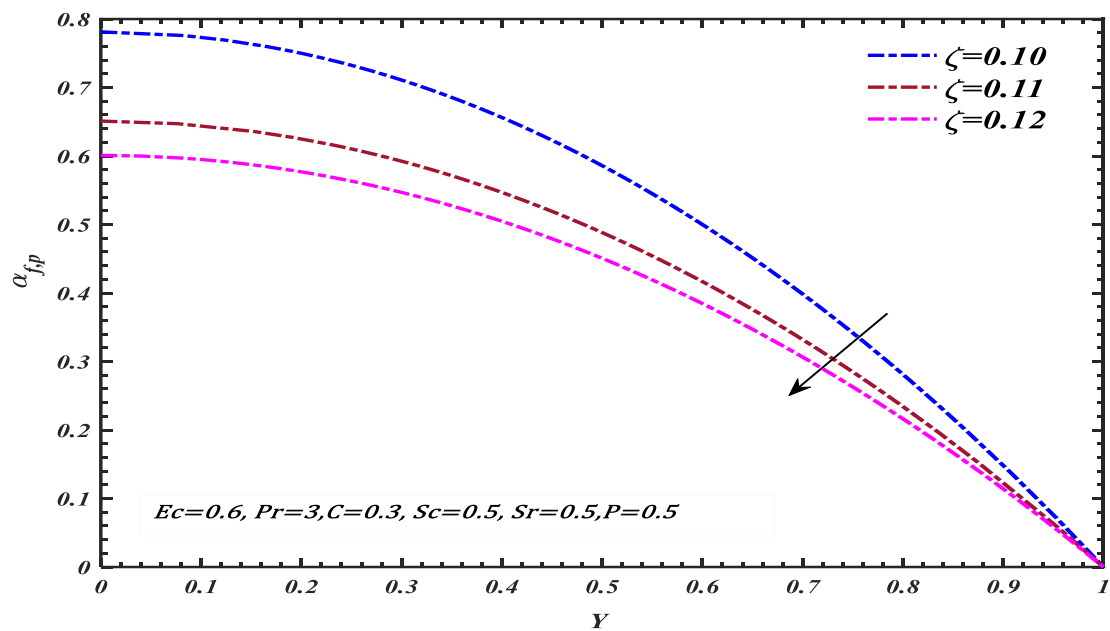


**Figure 9.** Impact of Saffman suspension parameter ( $\zeta$ ) on concentration  $(\alpha)_{f,p}$

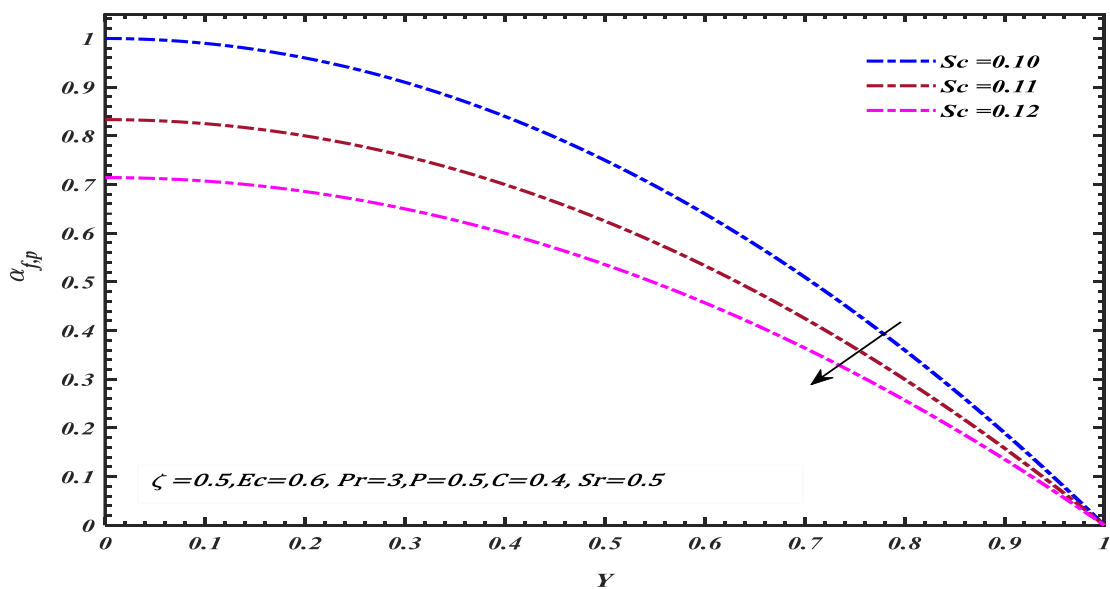


**Figure 10.** Impact of Schmidt number ( $Sc$ ) on concentration  $(\alpha)_{f,p}$

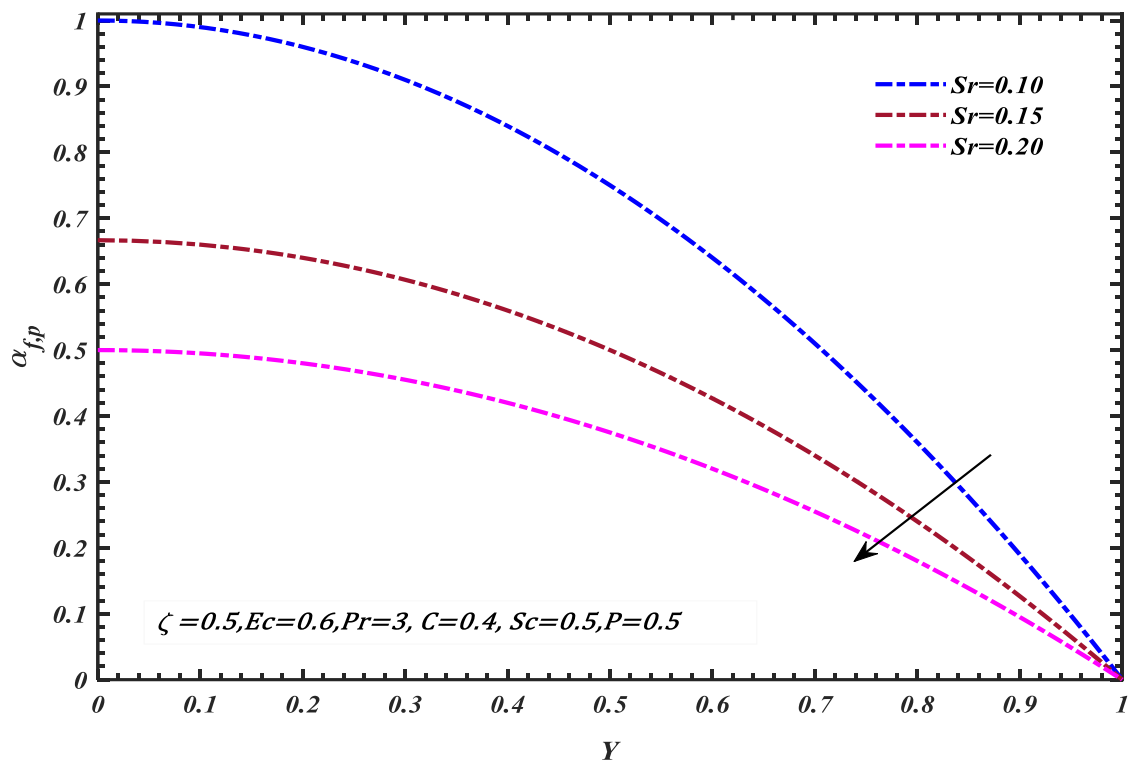


**Figure 11.** Impact of Soret number ( $Sr$ ) on concentration  $(\alpha)_{f,p}$

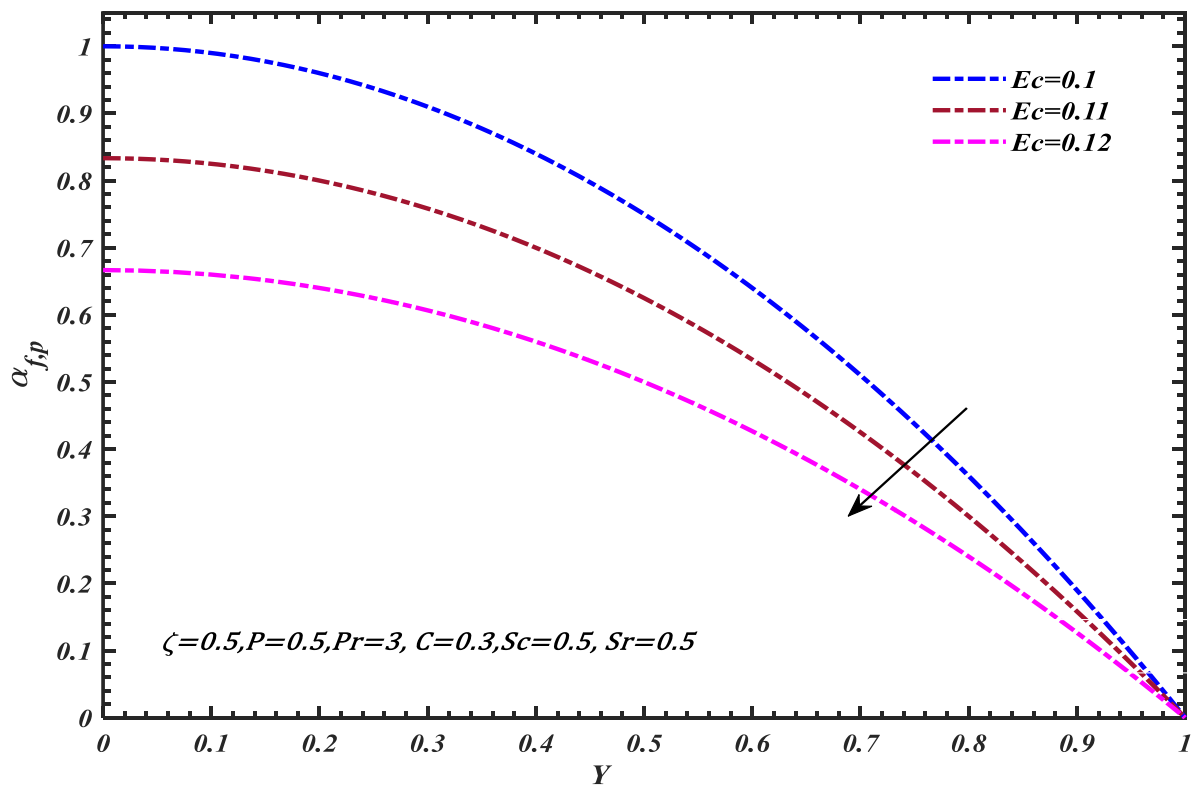


**Figure 12.** Impact of Eckert number ( $Ec$ ) on concentration  $(\alpha)_{f,p}$

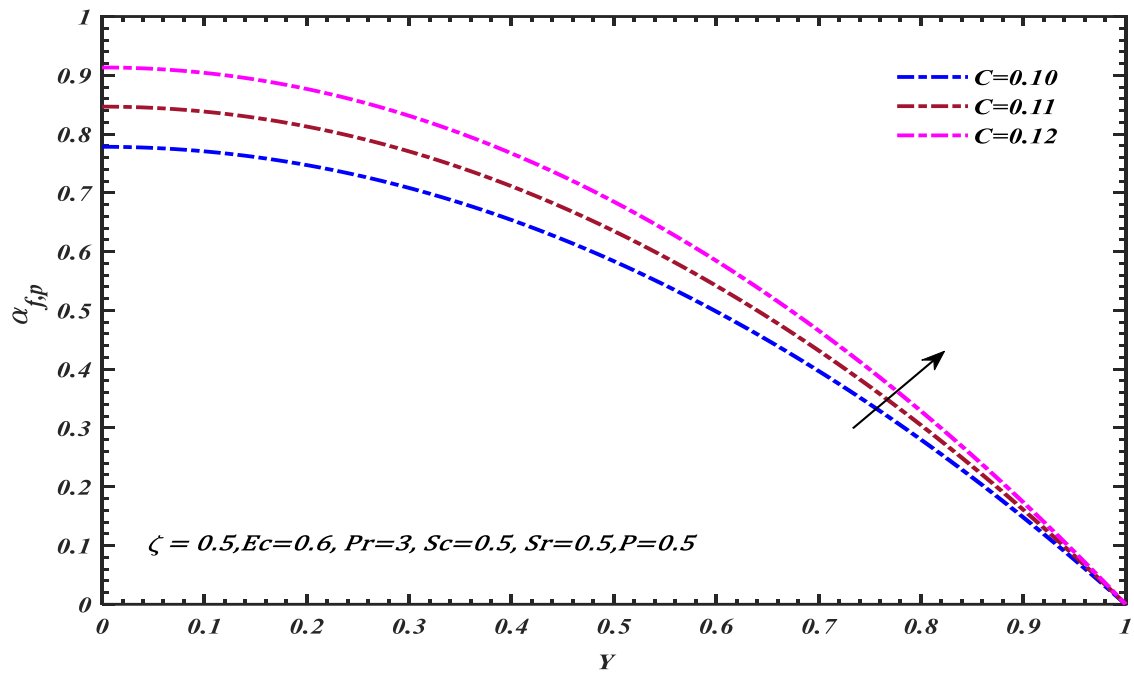


**Figure 13.** Impact of particle volume fraction ( $C$ ) on concentration ( $\alpha_{f,p}$ )

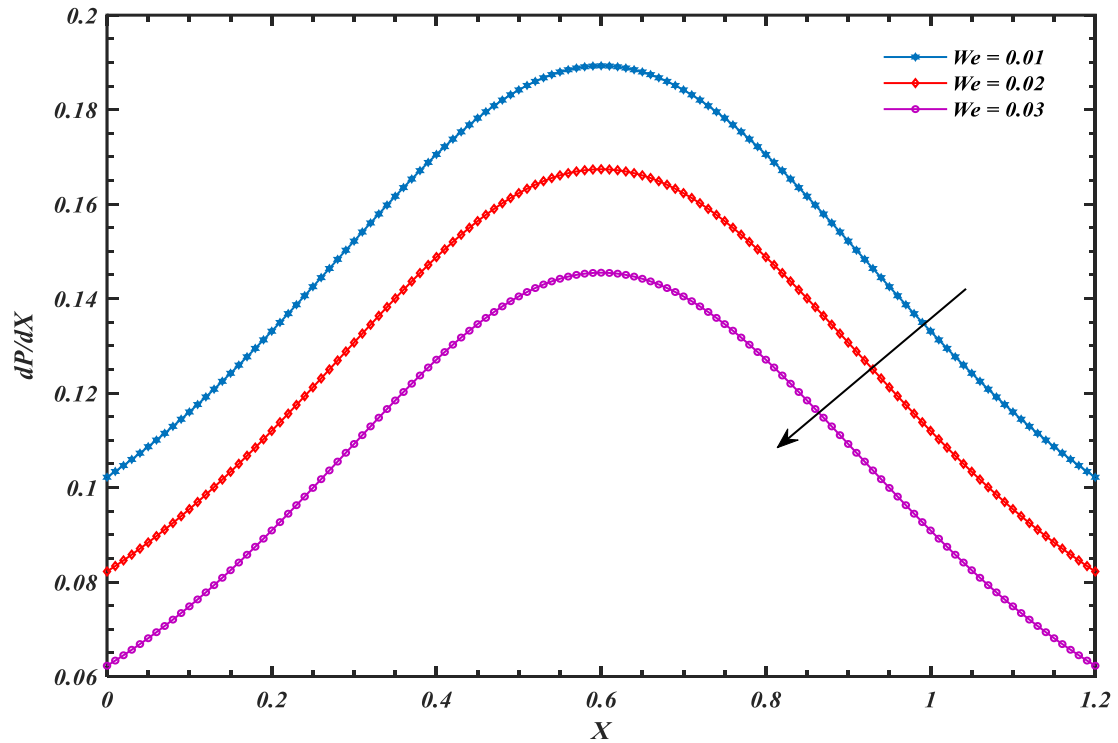


**Figure 14.** Impact of Weissenberg ( $We$ ) on pressure gradient ( $dP/dX$ )

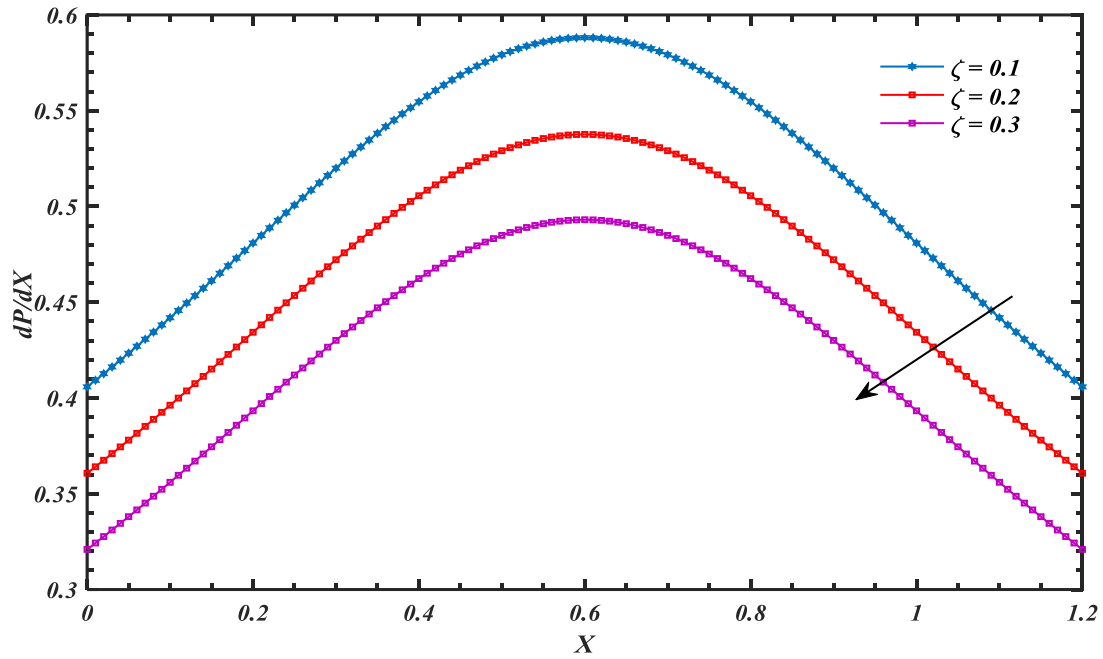


**Figure 15.** Impact of Suspension parameter ( $\zeta$ ) on pressure gradient ( $dP/dX$ )

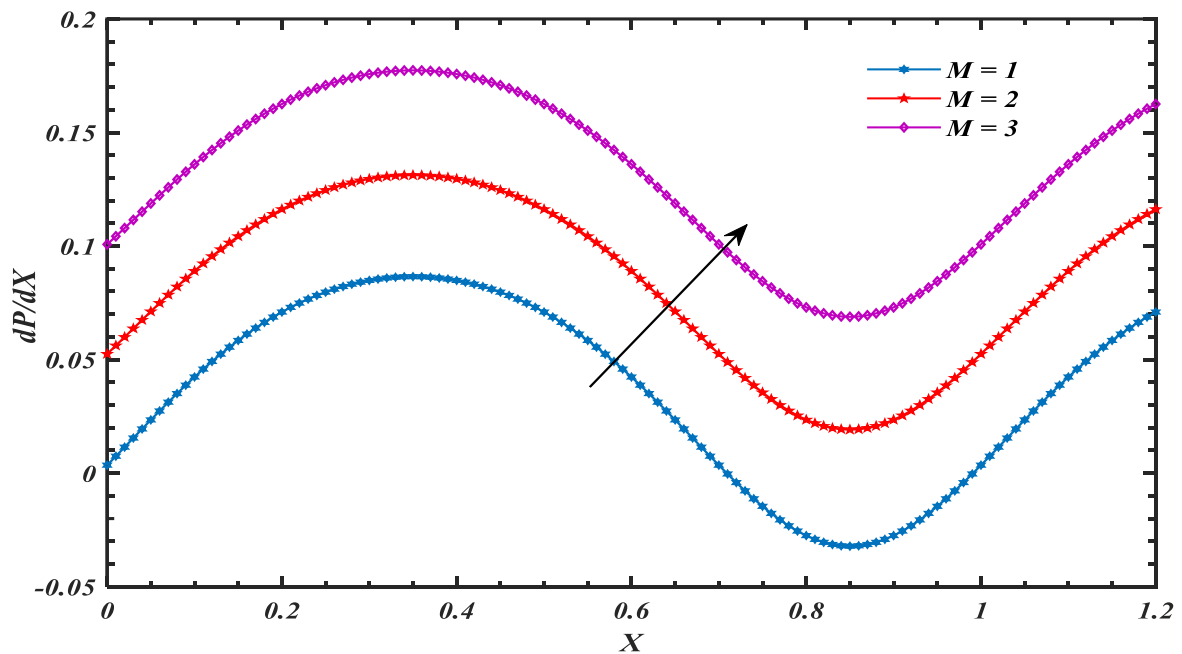


**Figure 16.** Impact of Hartmann number ( $M$ ) on pressure gradient ( $dP/dX$ )

#### 4.4. Local skin friction, local nusselt number and local sherwood number:

**Tables 1-2** display the physical meaning of local skin friction, local Nusselt number, and local Sherwood number in both the x and y axes. The **Table 1** displays the local axial and transverse skin frictions caused by the parameters  $\zeta$ , Ha, C, and We. The Williamson

parameter has an inverse relationship with the yield stress, resulting in increased viscosity at the surface and heightened axial skin friction. After examining **Table 1**, it is clear that the skin-friction coefficient shows a positive link with the increasing values of  $\zeta$ ,  $C$ ,  $Ha$ , and  $We$ . **Table 2** exposed to view the local Nusselt number for various combinations of  $C$  and  $Pr$ . The table includes four alternative values of the Prandtl number, specifically  $Pr=2, 5, 6,$  and  $7$ . Increasing the Prandtl number or thermal radiation leads to an increase in the rate of heat transfer, hence enhancing the local Nusselt number. Similar observations are made across the entire table for varying values of the remaining parameter. The Williamson parameters primarily affect the velocity profile, but have minimal impact on the local Nusselt number. An opposite phenomenon is observed for the Schmidt and Soret number in **Table 2**, which decrease the local Sherwood number. The velocity slip plays a crucial role in determining the local Sherwood number, and it experiences a substantial drop.

**Table 1.** The fluctuation of local skin friction number for specific values  $\zeta, Ha, C$  and  $We$ .

<b>Local Skin friction</b>				
$\zeta$	$Ha$	$C$	$We$	<i>Skin friction</i>
0.01	2.23	0.4	0.2	0.045
0.02				0.057
0.03				0.0675
0.04				0.0944
0.02	1	0.4	0.2	0.055
	2			0.0892
	3			0.0939
	4			0.1024
0.02	1	0	0.3	0.0357
		0.1		0.0578
		0.2		0.0827
		0.3		0.1265
0.02	1	0.3	1	0.0364
			3	0.693
			5	0.0875
			7	0.112

**Table 2.** The fluctuations of local Nusselt and Sherwood numbers for specific values  $C$ ,  $Pr$ ,  $Sc$  and  $Sr$ .

Local Nusselt Number and Sherwood number					
$C$	$Pr$	$Sc$	$Sr$	Nusselt Number	Sherwood number
0.1	0.2			0.0768	
0.2				0.096	
0.3				0.1152	
0.3	2			0.0461	
	5			0.0691	
	7			0.1613	
		0.1			0.7199
		0.2			0.6746
		0.3			0.5178
			0.4		0.6126
			0.45		0.6092
			0.5		0.5264

## 5. Verification of Findings:

The acquired results are compared with the literature of Maraj et al [32] as a limiting case of the reported issue, and are found to be in excellent agreement, as shown in **Table 3**.

- i). This investigation may become a single-phase problem when volume fraction  $C$  equals zero.
- ii). The values almost coincide with existing literature.

**Table 3:** The acquired results are compared with the available literature [32], which serves as a limiting case for the topic being studied on velocity profile.

$We$	$C$	$\zeta$	$M$	Maraj et al. [32]	Present Study
0	0.3	0.2	0	0.1376	0.1399
0	0.4	0.2	0	0.1365	0.1388
0	0.5	0.2	0	0.1328	0.1331
0	0.5	0.3	0	0.1386	0.1429
0	0.5	0.6	0	0.1374	0.1418
0	0.5	0.9	0	0.1339	0.1385

The velocity by varying magnetic field is plotted in **Figure 17** and validated with previous results. Ongoing problem implies the flow of Williamson fluid in presence of magnetic field. Maraj *et al.* [32] solved and experienced with different non-Newtonian fluid in the absence of magnetic field. Based on this comparison, it is evident that the findings of this inquiry are accurate and provide robust and accurate simultaneous results.

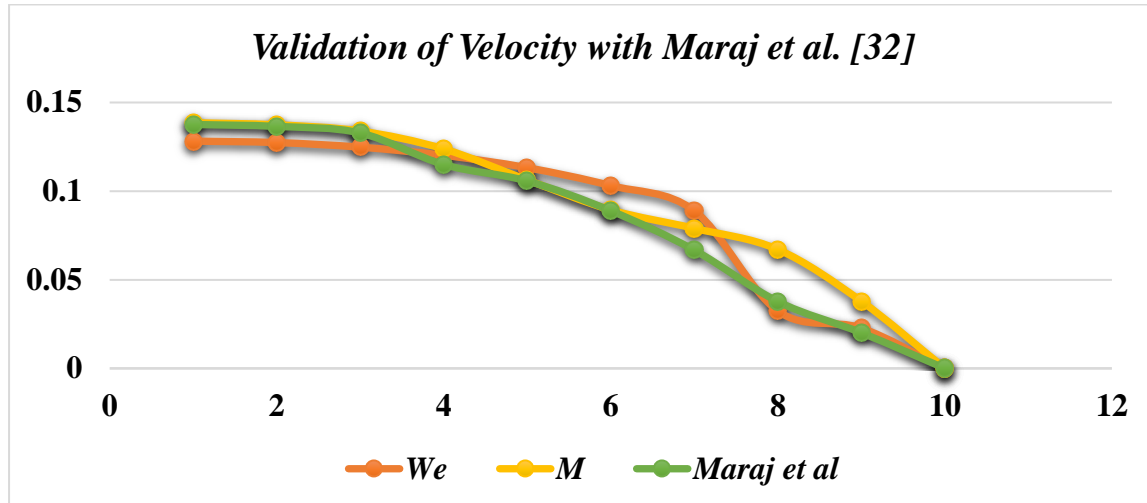


**Figure 17.** Validation of velocity parameters with Maraj *et al.* [32].

## 6. Conclusions

Motivated by emerging applications in electromagnetic ureteral flow therapy for combatting monoliths [57], a novel mathematical model in two phase flow [60] has been developed for simulating the two-dimensional, two-phase magnetohydrodynamic (MHD) [61] urological incompressible non-Newtonian peristaltic propulsion in the ureter under sinusoidal waves along the boundaries. Saffman's fluid-particle suspension model has been utilized. The Williamson viscoelastic model has been deployed for the rheology and heat transfer has also been incorporated in the model with Soret thermo-diffusion and viscous heating effects. Using long wave and low Reynolds number approximations (lubrication theory), the mass, momentum, energy, and concentration conservation equations with associated boundary conditions have been transformed to a non-dimensional boundary value problem. A numerical solution has been obtained via BVP4C MATLAB quadrature. Graphical visualizations of the velocity, temperature, and concentration (solid grains) have been presented for the influence of Saffman suspension parameter ( $\zeta$ ), Hartmann number ( $M$ ), Prandtl Number ( $Pr$ ), Weissenburg number ( $We$ ), particle volume fraction ( $C$ ), Eckert number ( $Ec$ ), Soret number ( $Sr$ ), Schmidt number ( $Sc$ ). The simulations have shown that:

- i). With greater magnetic field intensity i.e. greater Hartmann number, there is a strong suppression in the ureteral fluid phase velocity confirming the excellent flow control abilities of Magnetic Ureteral Therapy (MUT).
- ii). With elevation in Saffman suspension parameter,  $\zeta$  greater slip between the fluid and particles is produced which elevates fluid phase velocity magnitudes.
- iii). With increasing Weissenberg number ( $We$ ) i.e., stronger elastic force relative to viscous force in the rheological urodynamic fluid, a strong deceleration in the flow is computed.
- iv). A strong depletion in temperature in the fluid phase accompanies an increase in Prandtl number.
- v). Increasing particle volume fraction ( $C$ ) significantly reduces the fluid phase temperature whereas an increase in Eckert number and the Saffman suspension parameter ( $\zeta$ ) both generates temperature elevation in the peristaltic regime.
- vi). Increasing values of Saffman suspension parameter ( $\zeta$ ), Schmidt number ( $Sc$ ), Soret number ( $Sr$ ) and Eckert number ( $Ec$ ) all consistently induce a reduction in concentration magnitudes.

The present work has revealed some interesting insights into electromagnetic ureteral peristaltic multi-phase non-Newtonian thermo-solutal transport phenomena. Future studies may also consider visualization of the bolus dynamics and the deployment of electrical fields. Efforts in these directions are currently underway and will be reported imminently. It is also noteworthy that the renal pelvis plays a reservoir function role in urodynamics, and improved simulations of electromagnetic therapy may require computational fluid dynamics (CFD) software to capture all the complex characteristics including 3-D fluid-structure interaction with the viscoelastic ureteral wall, mural tension and mixing of contents as controlled by neurological functions. Excellent commercial software such as FREEFEM++ [58] and ANSYS FLUENT [59] are available for achieving this level of sophistication and are also currently being explored.

### **Conflict of Interest Statement**

The authors report no conflicts of interest.

### **References**

- [1] W.F. Dai, P. Wu and G.M. Liu, "A two-phase flow approach for modelling blood stasis and estimating the thrombosis potential of a ventricular assist device," *Int J Artif Organs*, vol. 44, no. 7, pp 471-480, 2021. [DOI: 10.1177/0391398820975405](https://doi.org/10.1177/0391398820975405).

- [2] I.D. Boutopoulos, D.S. Lampropoulos, G.C. Bourantas, K. Miller and V.C. Loukopoulos, “Two-phase biofluid flow model for magnetic drug targeting,” *Symmetry*, vol. 12, no. 7, pp 1083, 2020. DOI: [10.3390/sym12071083](https://doi.org/10.3390/sym12071083).
- [3] J. Dong, K. Inthavong and J. Tu, “Multiphase flows in biomedical applications”, *Handbook of Multiphase Flow Science and Technology*, 2020. DOI: [https://doi.org/10.1007/978-981-4585-86-6\\_16-1](https://doi.org/10.1007/978-981-4585-86-6_16-1).
- [4] S.A. Khashan, E.P. Furlani, “Coupled particle–fluid transport and magnetic separation in microfluidic systems with passive magnetic functionality,” *J. Phys. D Appl. Phys.*, vol. 46, no. 12, pp. 125002, 2013. DOI: [10.1088/0022-3727/46/12/125002](https://doi.org/10.1088/0022-3727/46/12/125002).
- [5] J. R. Levick, J. N. McDonald, “Fluid movement across synovium in healthy joints: role of synovial fluid macromolecules,” *Annals of the Rheumatic Diseases*, vol. 54, no. 5, pp. 417-423, 1995. DOI: [10.1136/ard.54.5.417](https://doi.org/10.1136/ard.54.5.417).
- [6] T. A. Béq, M.M. Rashidi, O. Anwar Béq and N. Rahimzadeh, “Differential transform semi-numerical simulation of biofluid-particle suspension flow and heat transfer in non-Darcian porous media,” *Computer Methods Biomechanics Biomedical Engineering*, vol. 16, no. 8, pp. 896-907, 2013. DOI: [10.1080/10255842.2011.643470](https://doi.org/10.1080/10255842.2011.643470).
- [7] J. R. Levick, “An analysis of the interaction between extravascular plasma protein, interstitial flow and capillary filtration; application to synovium,” *Microvasc Res.*, vol. 47, no. 1, pp. 90-125, 1994. DOI: [10.1006/mvre.1994.1007](https://doi.org/10.1006/mvre.1994.1007).
- [8] O.A. Béq, M.M. Rashidi, N. Rahimzadeh, T.A. Beg, T.K. Hung, “Homotopy semi-numerical simulation of two-phase thermal haemodynamics in a high permeability blood purification device,” *J. Mechanics Medicine and Biology*, vol. 13, no. 4, pp. 1350066, 2013. DOI: [10.1142/S0219519413500668](https://doi.org/10.1142/S0219519413500668).
- [9] K. Aukland, R.K. Reed, “Interstitial-lymphatic mechanisms in the control of extracellular fluid volume,” *Physiol Rev.*, vol. 73, no. 1, pp. 1-78, 1993. DOI: [10.1152/physrev.1993.73.1.1](https://doi.org/10.1152/physrev.1993.73.1.1).
- [10] O.A. Beg, M.M. Rashidi, M. Akbari, A. Hosseini, “Comparative numerical study of single-phase and two-phase models for bio-nanofluid transport phenomena,” *J. Mechanics in Medicine and Biology*, vol. 14, pp. 1450011.1-31 (2014). DOI: [10.1142/S0219519414500110](https://doi.org/10.1142/S0219519414500110).
- [11] M.M. Bhatti, A. Zeeshan, R. Ellahi, O.A. Béq and A. Kadir, “Effects of coagulation on the two-phase peristaltic pumping of magnetized Prandtl biofluid through an endoscopic annular geometry containing a porous medium,” *Chinese J. Physics*. vol. 58, pp. 222-234, 2019. DOI: <https://doi.org/10.1016/j.cjph.2019.02.004>.
- [12] Rajesh Kumar Chandrawat, Varun Joshi and O. Anwar Béq, “Numerical study of time-dependent flow of immiscible Saffman dusty (fluid-particle suspension) and Eringen micropolar fluids in a duct with a modified cubic B-spline differential quadrature method,” *Int. Comm. Heat Mass Transfer*. Vol. 130, 105758, 2022. (18 pages). DOI: [doi.org/10.1016/j.icheatmasstransfer.2021.105758](https://doi.org/10.1016/j.icheatmasstransfer.2021.105758)
- [13] J.M. Mansour and V.C. Mow, “On the natural lubrication of synovial joints: normal and degenerate,” *ASME J. of Lubrication Tech*, Vol. 99, no. 2, pp. 163-172, 1977. DOI: <https://doi.org/10.1115/1.3453003>.
- [14] J. Reynard, SF. Brewster, S. Biers, NL. Neal, *Oxford Handbook of Urology* (3 edn), Oxford University Press, 2013.

- [15] Paul A. Bergamin and Anthony J. Kiosoglous, “Surgical management of recurrent urinary tract infections: a review,” *Transl Androl Urol.* 2017, Vol. 6, no. 2, pp. S153–S162. DOI: <http://dx.doi.org/10.21037/tau.2017.06.17>.
- [16] A. L. Doukkali, “A hybrid individual-based mathematical model to study bladder infections,” *Front. Appl. Math. Stat., Mathematical Biology*, Vol. 9, 2023. DOI: <https://doi.org/10.3389/fams.2023.1090334>.
- [17] Y. C. Fung, C. S. Yih, “Peristaltic transport.” *ASME J. Appl. Mech.* Dec 1968, Vol. 35, no. 4, pp. 669-675, 1968. DOI: <https://doi.org/10.1115/1.3601290>
- [18] Shapiro, A. H., Jaffrin, M. Y., Weinberg, S. L.: Peristaltic pumping with long wavelengths at low Reynolds number. *J. Fluid Mechanics* 37, 799 (1969). DOI:
- [19] Lykoudis, P.S.: The ureter as a peristaltic pump, *Chapt. 16, Urodynamics, Hydrodynamics of the Ureter and Renal Pelvis*. New York: Academic Press (1971). DOI:
- [20] S. Boyarsky and S. Weinberg, Urodynamics Concepts, in *W. Lutzeyer et al. (eds.), Urodynamics*, Springer-Verlag Berlin · Heidelberg, Germany (1973). DOI:
- [21] Lozano, J.N.J.: Peristaltic flow with application to ureteral biomechanics, *PhD Thesis, University of Notre Dame, Indiana, USA*. (2009). DOI:
- [22] Kiil, F.: Urinary flow and ureteral peristalsis. In: *Lutzeyer, W., Melchior, H. (eds) Urodynamics*, pp. 57-70. Springer, Heidelberg (1973). DOI:
- [23] Vahidi, B., Fatourae, N., Imanparast, A., Moghadam, A.N.: A mathematical simulation of the ureter: effects of the model parameters on ureteral pressure/flow relations. *ASME J Biomech Eng.* 133, 031004 (2011). DOI: <https://doi.org/10.1115/1.4003316>.
- [24] J. Carlos Gómez-Blanco *et al.*, Fluid structural analysis of urine flow in a stented ureter, *Comput Math Methods Med.* 2016; 2016: 5710798. DOI:
- [25] P.G. Saffman, On the stability of laminar flow of a dusty gas, *J. Fluid Mechanics*, 13, 120-128 (1962). DOI:
- [26] Marble, F.E., Dynamics of dusty gases, *Ann. Rev. Fluid Mech.*, 2: 397- 446 (1970). DOI:
- [27] Srivastava, L. M., Srivastava, V. P.: Peristaltic transport of a particle-fluid suspension. *ASME. J Biomech Eng.* 111, 157–165 (1989). DOI: <https://doi.org/10.1115/1.3168358>
- [28] Kamel, M. H., Eldesoky I.M., Maher B.M., Abumandour R.M.: Slip effects on peristaltic transport of a particle-fluid suspension in a planar channel. *Appl. Bionics Biomech.* 2015, 1-14 (2015). DOI: <https://doi.org/10.1155/2015/703574>
- [29] M.M. Bhatti, A. Zeeshan, Heat and mass transfer analysis on peristaltic flow of particle-fluid suspension with slip effects, *J. Mech. Med. Biol.*, 17 (2012), Article 1750028 DOI:
- [30] Misra, J. C., Pandey S. K.: Peristaltic transport of a particle-fluid suspension in a cylindrical tube, *Comput. Math. Appl.* 28, 131-145, (1994). DOI: [https://doi.org/10.1016/0898-1221\(94\)00134-0](https://doi.org/10.1016/0898-1221(94)00134-0)
- [31] Mohd Kasim, A.R., Arifin, N.S., Mohd Zokri, S., Salleh, M.Z., Mohammad, N.F., Chuan Ching, D.L., Shafie, S., Ariffin, N.A.N. Convective transport of fluid–solid interaction: a study between non-Newtonian Casson model with dust particles. *Crystals.* 10, 814 (2020). DOI: <https://doi.org/10.3390/cryst10090814>
- [32] Maraj, E. N., Shah, S. I., Akbar, N. S., Muhammad, T.: Thermally progressive particle-cu/blood peristaltic transport with mass transfer in a non-uniform wavy channel:

- closed-form exact solutions. *Alex. Eng. J.* 74, 453-466 (2023). DOI: <https://doi.org/10.1016/j.aej.2023.05.056>
- [33] Riaz, A., Sadiq, M. A.: Particle–fluid suspension of a non-Newtonian fluid through a curved passage: an application of urinary tract infections. *Front. Phys.* 8, 109 (2020). DOI: <https://doi.org/10.3389/fphy.2020.00109>
- [34] Xiong, P. Y., Nazeer, M., Hussain, F., Khan, M. I., Saleem, A., Qayyum, S., Chu, Y. M.: Two-phase flow of couple stress fluid thermally effected slip boundary conditions: numerical analysis with variable liquids properties. *Alex. Eng. J.* 61, 3821-3830 (2022). DOI: <https://doi.org/10.1016/j.aej.2021.09.012>
- [35] Zhang, L., Bhatti, M. M., Michaelides, E. E.: Thermally developed coupled stress particle–fluid motion with mass transfer and peristalsis. *J. Therm. Anal. Calorim.* 143, 2515-2524 (2021). DOI: <https://doi.org/10.1007/s10973-020-09871-w>
- [36] A A Li, N I Nesterov, S N Malikova, V A Kiiatkin, The use of an impulse magnetic field in the combined therapy of patients with stone fragments in the upper urinary tract, *Vopr Kurortol Fizioter Lech Fiz Kult*, (3): 22-4 (1994). DOI:
- [37] <https://techfinder.stanford.edu/technology/magnetic-medical-device-efficient-removal-kidney-stones-during-ureteroscopy> (Magnetic medical device for efficient removal of kidney stones during ureteroscopy, Stanford University, California, USA) (2023).
- [38] Ramesh, K., Tripathi, D., Bég, O.A., Kadir, A.: Slip and Hall current effects on Jeffrey fluid suspension flow in a peristaltic hydromagnetic blood micropump. *Iran. J. Sci. Technol-Trans. Mech. Eng.* 43, 675–692 (2019). DOI: <https://doi.org/10.1007/s40997-018-0230-5>
- [39] Bhatti, M. M., Zeeshan, A., Ijaz, N., Bég, O. A., Kadir, A.: Mathematical modelling of nonlinear thermal radiation effects on EMHD peristaltic pumping of viscoelastic dusty fluid through a porous medium duct. *Eng. Sci. Technol.* 20, 1129-1139 (2017). DOI: <https://doi.org/10.1016/j.jestch.2016.11.003>
- [40] Nadeem, S., Safia Akram.: Peristaltic flow of a Williamson fluid in an asymmetric channel. *Commun Nonlinear Sci Numer Simul.* 15, 1705-1716 (2010) DOI: <https://doi.org/10.1016/j.cnsns.2009.07.026>
- [41] Jabeen, Kanwal, Muhammad Mushtaq, Tasmia Mushtaq, and Rana Muhammad Akram Muntazir, A numerical study of boundary layer flow of Williamson nanofluid in the presence of viscous dissipation, bioconvection, and activation energy. *Numerical Heat Transfer, Part A: Applications* 85, no. 3: 378-399, (2024). DOI:
- [42] G. Shankar, and E.P. Siva, “A Numerical Investigation of Thermal and Mass Exchange of Blood Along Porous Stenosis Arterial Flow with Applied Magnetic Field,” *IAENG Int. J. Appl. Math.*, vol. 54, no. 3, pp. 532-541, 2024.
- [43] G. Sutton and A. Sherman, *Engineering Magnetohydrodynamics*, MacGraw-Hill, New York, USA (1965). DOI:
- [44] Stanley Middleman, *An Introduction to Mass and Heat Transfer: Principles of Analysis and Design*, John Wiley, USA 704pp (1997). DOI:
- [45] Umavathi JC and Bég O. Anwar, Mathematical modelling of triple diffusion in natural convection flow in a vertical duct with Robin boundary conditions, viscous heating and chemical reaction effects. *J. Engineering Thermophysics.* 2020; 29:1–26. DOI:
- [46] Umavathi JC, Patil SL, Mahanthesh B and Bég O. Anwar. Unsteady squeezing flow of magnetized nano-lubricant between parallel disks with Robin boundary condition.

- Proc. IMechE J. Nanomaterials Nanoengineering, Nanosystems.* 2020; DOI: 10.1177/23977914211036562 (15 pages)
- [47] O. Anwar Bég, F.T. Zohra, M.J. Uddin, A. Ismail, S. Sathasivam, Energy conservation of nanofluids from a biomagnetic needle in the presence of Stefan blowing: Lie symmetry and numerical simulation, *Case Studies in Thermal Engineering*, Volume 24, 100861 (2021). DOI:
- [48] M. Waqas, O. Anwar Bég and S. Kuharat *et al.* Computation of SWCNT/MWCNT-doped thermo-magneto-nano-blood flow with chemical reaction from a stretching wall in a non-Darcy porous medium, *Int. J. Hydrogen Energy* (2023) (15 pages). DOI: doi.org/10.1016/j.ijhydene. 2023.05.036
- [49] K. Bhagya Swetha Latha, M. Gnaneswara Reddy, D. Tripathi, O. Anwar Bég, S. Kuharat, Computation of stagnation coating flow of electro-conductive ternary Williamson hybrid GO-Au-CO<sub>3</sub>O<sub>4</sub>/EO nanofluid with a Cattaneo-Christov heat flux model and magnetic induction, *Nature- Scientific Reports* (2023). 13, Article number: 10972 (2023) (26 pages). DOI:
- [50] J Prakash, H Upreti, D Tripathi, and A K Pandey, Irreversibility and heat transfer analysis in MHD Darcy-Forchheimer flow of Casson hybrid nanofluid flow through cone and wedge, *Numerical Heat Transfer, Part A: Applications*: 1-27, (2023). DOI:
- [51] R. Balaji, J. Prakash, Dharmendra Tripathi and O. Anwar Bég, Computation of of magnetohydrodynamic (MHD) electro-osmotic modulated rotating squeezing flow with zeta potential effects, *Colloids and Surfaces A: Physicochemical and Engineering Aspects* (2022). 128430. DOI: <https://doi.org/10.1016/j.colsurfa.2022.128430> (13 pages)
- [52] Kattan PI. *Matlab For Beginners*. CreateSpace Independent Publishing Platform; USA: 2008. DOI:
- [53] Brant A. Inman, Wiguins Etienne, Rainier Rubin, Richmond A. Owusu, Tiago R. Oliveira, Dario B. Rodrigues, Paolo F. Maccarini, Paul R. Stauffer, Alireza Mashal & Mark W. Dewhirst (2013) The impact of temperature and urinary constituents on urine viscosity and its relevance to bladder hyperthermia treatment, *International Journal of Hyperthermia*, 29:3, 206-210, DOI: 10.3109/02656736.2013.775355.
- [54] Ohlson, L., 1989, Morphological dynamics of ureteral transport I. Shape and volume of constituent urine fractions, *Am. J. Physiol.*, 256, pp. R19-R28. DOI:
- [55] Ohlson, L., 1989, Morphological dynamics of ureteral transport II. Peristaltic patterns in relation to flow rate, *Am. J. Physiol.*, 256, pp. R29-R34. DOI:
- [56] Roselli R, Diller K. *Biotransport: Principles and Applications*. New York: Springer (2011). DOI:
- [57] A. Lonappan, V. Hamsakkutty, G. Bindu, J. Jacob, V. Thomas, K.T. Mathew, “Dielectric properties of human urine at microwave frequencies,” *Microwave and Optical Technology Letters*, vol. 42, no. 6, pp. 500-503, 2004. DOI: 10.1002/mop.20349.
- [58] B. Vasu, A. Dubey, O.A. Bég, R.S.R. Gorla Vasu, “Micropolar pulsatile blood flow conveying nanoparticles in a stenotic tapered artery: non-Newtonian pharmacodynamic simulation,” *Computers in Biology and Medicine*, vol. 126, pp. 104025, 2020. DOI: 10.1016/j.compbiomed.2020.104025.
- [59] K. Choglay, O. Anwar Bég, S. Kuharat and A. Kadir, “Enhancing Pharmacological Applications: Investigating Convective Heat Transfer in Nanoparticles within Blood

- Flow through CFD Simulation using ANSYS FLUENT,” *Glasgow University Computational Biology Conference*, 2023.
- [60] M.W. Waite, “Numerical investigation of two-phase fluid flow and heat transfer in porous media heated from the side,” *Numerical Heat Transfer: Part A: Applications*, vol. 35, no. 3, pp. 271-290, 1999. DOI: [10.1080/104077899275245](https://doi.org/10.1080/104077899275245).
- [61] O. Prakash, P. Barman, P.S. Rao and R.P. Sharma Prakash, “MHD free convection in a partially open wavy porous cavity filled with nanofluid,” *Numerical Heat Transfer, Part A: Applications*, vol. 84, no. 5, pp. 449-463, 2023. DOI: [10.1080/10407782.2022.2132330](https://doi.org/10.1080/10407782.2022.2132330).
- [62] M. Ajithkumar, P. Lakshminarayana, and K. Vajravelu, “Diffusion effects on mixed convective peristaltic flow of a bi-viscous Bingham nanofluid through a porous medium with convective boundary conditions,” *Physics of Fluids*, vol. 35, no. 3, 2023. DOI:10.1063/5.0142003.
- [63] M. Ajithkumar, P. Lakshminarayana and K. Vajravelu, “Peristaltic transport of MHD Ree–Eyring fluid through a flexible channel under the influence of activation energy,” *Physics of Fluids*, vol. 35, no. 6, 2023. DOI:10.1063/5.0153716.
- [64] M. Ajithkumar, P. Lakshminarayana and K. Vajravelu, “Peristaltic flow of bioconvective Ree–Eyring nanofluid through an inclined elastic channel with partial slip effects,” *Journal of Applied Physics*, vol. 134, no. 15, 2023. DOI: 10.1063/5.0171422.
- [65] K. Vajravelu, S. Sreenadh and P. Lakshminarayana, “The influence of heat transfer on peristaltic transport of a Jeffrey fluid in a vertical porous stratum,” *Communications in Nonlinear Science and Numerical Simulation*, vol. 16, no. 8, pp. 3107-3125, 2011. DOI: 10.1016/j.cnsns.2010.11.001
- [66] M. Ajithkumar and P. Lakshminarayana, “MHD peristaltic flow of chemically reactive casson nanofluid in a nonuniform porous inclined flexible channel with cross-diffusion effects,” *International Journal of Modern Physics B*, vol. 37, no. 25, pp. 2350292, 2023. DOI:10.1142/S0217979223502922.
- [67] V. Jagadesh, S. Sreenadh, M. Ajithkumar, P. Lakshminarayana and G. Sucharitha, “Investigation of dissipative heat transfer and peristaltic pumping on MHD Casson fluid flow in an inclined channel filled with porous medium,” *Numerical Heat Transfer, Part B: Fundamentals*, pp. 1-19, 2023. DOI: 10.1080/10407790.2023.2269608.
- [68] M. Ajithkumar, K. Vajravelu, G. Sucharitha and P. Lakshminarayana, “Peristaltic flow of a bioconvective sutterby nanofluid in a flexible microchannel with compliant walls: Application to hemodynamic instability,” *Physics of Fluids*, vol. 35, no. 12, 2023. DOI:10.1063/5.0178766
- [69] M. Ajithkumar and P. Lakshminarayana, “Chemically reactive MHD peristaltic flow of Jeffrey nanofluid via a vertical porous conduit with complaint walls under the effects of bioconvection and double diffusion,” *International Journal of Modern Physics B*, pp. 2450203. 2023. DOI: 10.1142/S0217979224502035.
- [70] S.M. Kayani, S. Hina and M. Mustafa Kayani, “A new model and analysis for peristalsis of Carreau–Yasuda (CY) nanofluid subject to wall properties,” *Arabian Journal for Science and Engineering*, vol. 45, pp.5179-5190, 2020. DOI: 10.1007/s13369-020-04359-z.
- [71] S. Hina, S.M. Kayani and M. Mustafa, “Aiding or opposing electro-osmotic flow of Carreau–Yasuda nanofluid induced by peristaltic waves using Buongiorno model,”

- Waves in Random and Complex Media*, pp. 1-17, 2022, DOI:10.1080/17455030.2021.2024299.
- [72] M. Yasin, S. Hina and R. Naz, "Influence of inclined magnetic field on peristaltic flow of Ag–Cu/blood hybrid nanofluid in the presence of homogeneous–heterogeneous reactions with slip condition," *Arabian Journal for Science and Engineering*, vol. 48, no. 1, pp. 31-46, 2023. DOI:10.1007/s13369-022-06942-y.
- [73] M Yasin, S Hina and R Naz, "A modern study on peristaltically induced flow of Maxwell fluid considering modified Darcy's law and Hall effect with slip condition," *Alexandria Engineering Journal*, vol. 76, pp.835-850, 2023. DOI: 10.1016/j.aej.2023.06.074.